PALEONTOLOGY

Ultrastructure reveals ancestral vertebrate pharyngeal skeleton in yunnanozoans

Qingyi Tian[1,2], Fangchen Zhao[2]*, Han Zeng[2], Maoyan Zhu[2,3], Baoyu Jiang[1]*

Pharyngeal arches are a key innovation that likely contributed to the evolution of the jaws and braincase of vertebrates. It has long been hypothesized that the pharyngeal (branchial) arch evolved from an unjointed cartilaginous rod in vertebrate ancestors such as that in the nonvertebrate chordate amphioxus, but whether such ancestral anatomy existed remains unknown. The pharyngeal skeleton of controversial Cambrian animals called yunnanozoans may contain the oldest fossil evidence constraining the early evolution of the arches, yet its correlation with that of vertebrates is still disputed. By examining additional specimens in previously unexplored techniques (for example, x-ray microtomography, scanning and transmission electron microscopy, and energy dispersive spectrometry element mapping), we found evidence that yunnanozoan branchial arches consist of cellular cartilage with an extracellular matrix dominated by microfibrils, a feature hitherto considered specific to vertebrates. Our phylogenetic analysis provides further support that yunnanozoans are stem vertebrates.

Debate over the origin and early evolution of vertebrates revolves around the pharynx (*1*–*4*), but there is little high-resolution information available in the critical part of the vertebrate tree—its stem (*5*). Yunnanozoans from the early Cambrian Chengjiang fauna (~518 million years old) of China (*6*) are the oldest relatives of crown-group vertebrates, although their phylogenetic position remains sharply debated—they have been variously classified as stem vertebrates, cephalochordates, hemichordates, or even stem deuterostomes on the basis of disputed anatomical interpretations (*7*–*13*). Three species have been erected in the clade, *Yunnanozoon lividum* Hou, Ramsköld, and Bergström, 1991 (*7*), *Haikouella lanceolata* Chen, Huang, and Li, 1999 (*10*), and *H. jianshanensis* Shu *et al*., 2003 (*11*), but the latter two species were subsequently revised as junior synonyms of *Y. lividum* (*13*) (Fig. 1, A and B). This revised classification is adopted in this paper. Seven pairs of bilaterally symmetrical branchial arches have long been recognized in the pharynx of yunnanozoans (Fig. 1C). The first pair of mouth-surrounding arches were once interpreted as blood vessels in the upper and lower lips (*10*, *12*) or oral skirts (*11*), but others have argued for their close similarity to the remaining arches (*13*). Each branchial arch consists of a bamboo-like bar formed by evenly spaced, transverse septa and two rows of lanceolate gill filaments that attach to both sides of each segment (fig. S1B) (*10*). The stacked discoid structures in the bamboo-like bar were compared to those in the cellular cartilages of embryonic vertebrates (*8*, *10*), but this claim lacks further anatomical support (*12*). The arches attach to slightly bent horizontal rods at both their dorsal and ventral ends (*8*, *11*). The dorsal and ventral horizontal rods were previously interpreted as blood vessels, margins of the endostyle trough, or simply folds (*8*, *11*, *12*, *14*). These debates call for further study based on new specimens. Here, we reexamine the pharyngeal skeleton of yunnanozoans on the basis of 127 newly collected specimens and provide high-resolution anatomical and ultrastructural correlation with that of vertebrates.

Newly collected specimens confirm that the branchial arches comprise bamboo-like bars and lanceolate gill filaments (Fig. 1, D to F, and fig. S1, A and B). Dorsoventrally preserved specimens show that the gill filaments are external to the bars (Fig. 1H and fig. S5, B, D, and G). All the bars consist of ~25 straight, first-order septa that form a series of stacked discoid structures measuring ~170 μm wide and 140 μm thick (Fig. 1, D and E, and fig. S1B). Each discoid structure is subdivided into two to four cellular chambers by irregular second-order septa (N = 1 to 3) between the two neighboring first-order septa, which are straight and regularly organized (Fig. 1, D and E). X-ray computed microtomography (micro-CT) of two different animals reveals that the cellular chambers are 23 to 84 μm in diameter (N = 43) (Fig. 2 and fig. S2).

The arches are the most commonly preserved structures in yunnanozoans (*11*), with abundant carbonaceous residues (Fig. 3I and fig. S3, N, O, and Q). Under scanning electron microscopy (SEM), these residues comprise microfibrils that are thin, slightly wavy, largely parallel, and densely packed (Fig. 3, D and F, and fig. S3). Locally, the microfibrils are connected by short, parallel cross-linkages forming a lattice (Fig. 3F and fig. S3I). The microfibrils are extremely fine, best measured with transmission electron microscopy to be 12 ± 2 nm in diameter (N = 16) (Fig. 3, G and H). Carbonaceous particles locally aggregate forming a "beads-on-a-string" appearance with 50- to 60-nm intervals (Fig. 3H).

We sought and found the first branchial arch, lateral to a stout, dark circumoral structure (description is given in the supplementary text section of the supplementary materials) at the rostral end of the body. The first branchial arch is often fully or partly obscured by the underlapping circumoral structure, but close inspection reveals that the first arch, identical to the remaining arches, has bamboo-like segments delineated by first-order septa (fig. S1, F, L, and M), attached gill filaments (fig. S1, D, F, and H), and microfibrils in its matrix (fig. S3, C and D).

The seven branchial arches are aligned subparallel to each other and slightly inclined toward the rostral end (Fig. 1, C and F). The arches are connected by dorsoventrally curved, parenthesis-shaped horizontal rods at both ends (Fig. 1, F to H, and figs. S4 and S5; see also figure 16 in (*13*); measurements are given in supplementary text). These dorsal and ventral horizontal rods run subparallel to each other through most of the length of the pharynx then gradually converge between the seventh pair of arches and the gonads (fig. S5H). Locally, the rods show poorly preserved, putative bamboo-like structures (figs. S4D and S5, F and G). No gill filaments occur on the rods, but their matrix does contain microfibrils, as in the branchial arches (fig. S3S). The branchial bars articulate with the horizontal rods at joints, evidenced by the common presence of disarticulation between the two structures (figs. S1I and S5F). The horizontal rods are not to be confused with nearby dark lines called ventral and dorsal thin horizontal lines ("vtl" in fig. S5, B, C, and G; and "dtl" in fig. S1, K and N). These thinner lines might be longitudinal blood vessels, because they occur in the regions of the aortae of vertebrates (*10*–*12*).

Our findings can be interpreted in a comparative biological context. In vertebrates, chondrocytes are stacked parallel to the arch axis during chondrogenesis, forming the classical stacked discoid structures of pharyngeal arches in extant vertebrates (*15*, *16*). The arrangement, size, shape, and number of cellular chambers in the branchial bars of yunnanozoans match the chondrocytes in the pharyngeal arches of embryonic and primitive vertebrates and in the oral cirri of cephalochordates (Fig. 4D).

The microfibrils in the branchial arches of yunnanozoans have characteristics of fibrillin microfibrils, including their diameter of ~12 nm (*17*, *18*), wavy appearance, parallel bundling, and cross-linkages (*19*). They differ notably

[1]State Key Laboratory for Mineral Deposits Research, School of Earth Sciences and Engineering and Frontiers Science Center for Critical Earth Material Cycling, Nanjing University, Nanjing 210023, China. [2]State Key Laboratory of Palaeobiology and Stratigraphy, Nanjing Institute of Geology and Palaeontology and Center for Excellence in Life and Palaeoenvironment, Chinese Academy of Sciences, Nanjing 210008, China. [3]College of Earth and Planetary Sciences, University of Chinese Academy of Sciences, Beijing 100049, China.
*Corresponding author. Email: fczhao@nigpas.ac.cn (F.Z.); byjiang@nju.edu.cn (B.J.)

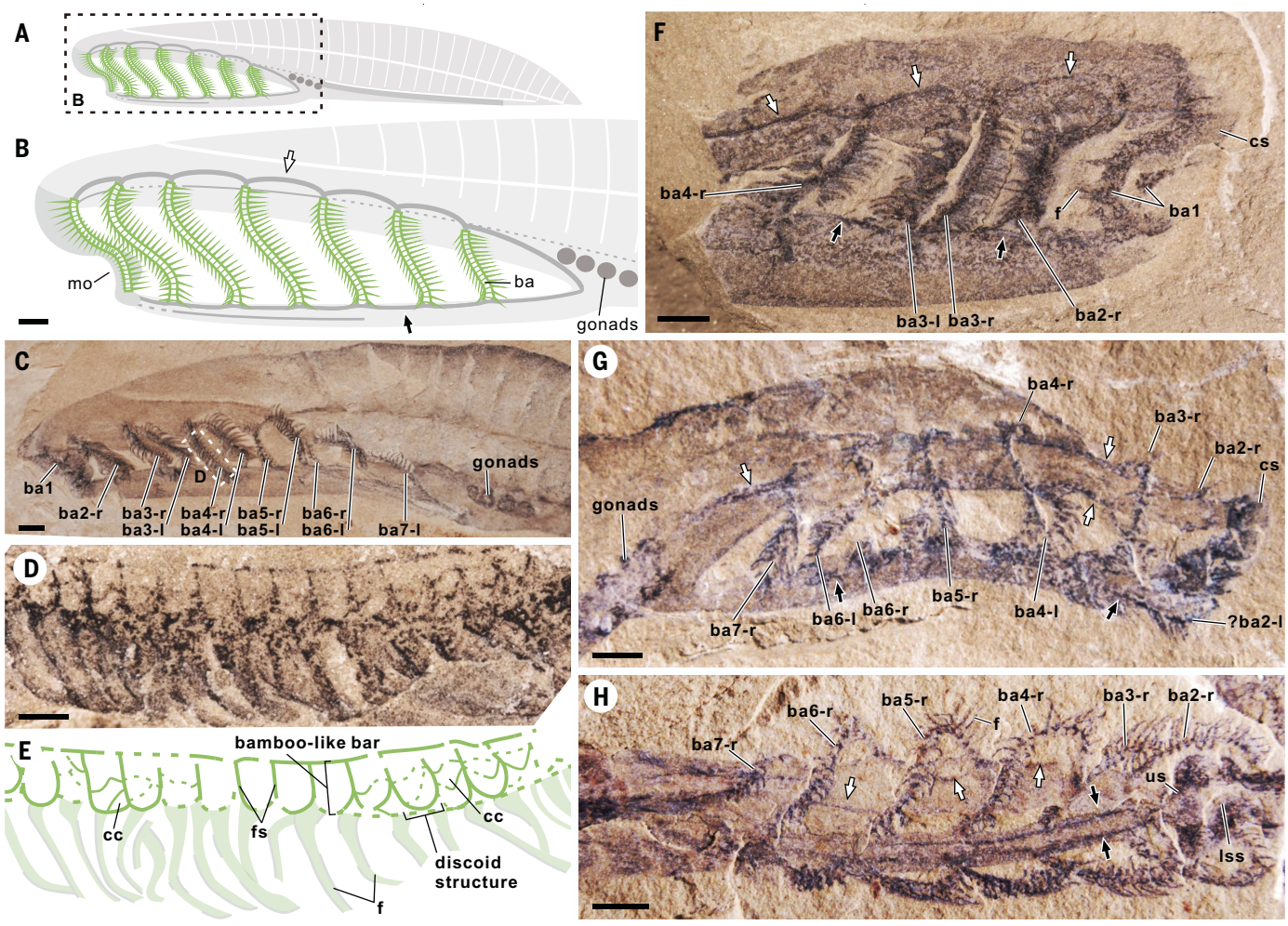

Fig. 1. Pharyngeal structures of yunnanozoans. (**A** and **B**) Line drawings of a yunnanozoan (A) and its pharynx (B). (**C** to **E**) An overview of the branchial arches in specimen NIGP 176256a (C). An enlargement (D) and line drawing (E) of the boxed area in (C) show detailed anatomy of each arch. (**F** to **H**) Lateral [(F) and (G)] and ventral views (H) show the dorsoventrally curved, parenthesis-shaped, horizontal rods in both the dorsal (white arrows) and ventral (black arrows) sides in specimens NIGP 176267a (F), EC00086a (G), and EC00308a (H). Abbreviations: ba1–7, branchial arches 1 to 7 (with "-r" and "-l" meaning right and left, respectively); cc, cellular chamber; cs, C-shaped structure; f, filament; fs, first-order septa; lss, lobe-shaped structure; mo, mouth opening; us, U-shaped structure. Scale bars: 1 mm in (B), (C), and (F) to (H); and 200 μm in (D).

from collagen fibrils, which have thicker diameters ranging from 20 to 500 nm and repeating banding patterns (every ~67 nm) instead of beads (*20*). Unlike collagen fibrils that are the major component of cartilages in jawed vertebrates (gnathostomes) (*20*, *21*), fibrillin microfibrils are the dominant extracellular matrix in some parts of cyclostome skeletons. The prominent examples occur in the first two pharyngeal arches of larval lampreys (*17*) and in the posterior lingual cartilage of a hagfish (*18*). Similar matrix microfibrils also characterize the pharyngeal skeletons of extant cephalochordates (*21*). The common presence of microfibrils further confirms that yunnanozoan branchial arches are cartilaginous, and this cartilage shares both anatomical and ultrastructural characteristics with that of primitive vertebrates and cephalochordates. The attached gill filaments with matrix microfibrils (fig. S3I) are possibly cartilaginous gill ray–like structures, as previously interpreted (*12*).

Turning next to the horizontal rods that connect the branchial arches in yunnanozoans: The presence of the microfibrils and putative septa again indicate their cartilaginous nature. As skeletal elements, the horizontal rods perhaps compare to the subchordal and hypobranchial bars in the branchial basket of lampreys (Fig. 4, B and C) (*15*). Comparable horizontal elements also existed in the stem hagfish *Myxinikela* (*22*) and the fossil jawless fish *Euphanerops* (*23*).

These new findings reveal that the branchial skeleton of yunnanozoans shares three characteristics broadly present in crown-group vertebrates: dominance of microfibrils in the matrix of a cartilage with chondrocytes, branchial arches with stacked discoid structures, and presence of the horizontal bars at both ends of the branchial arches. We ran phylogenetic analyses on a newly combined set of characters, both without and with the character modifications demanded by the findings of this study (fig. S6). These analyses support that yunnanozoans are the earliest branching stem vertebrates (Fig. 4A and fig. S6B).

The branchial arches of yunnanozoans also shed light on the early evolution of the vertebrate pharyngeal arches. Because the first arch in yunnanozoans is lateral to the circumoral structure and identical to the remaining arches, it completes a serial pattern of similar arches that is also seen in another stem vertebrate, *Metaspriggina* (Fig. 4) (*5*). Yunnanozoans are consistent with the conventional hypothesis that every pharyngeal

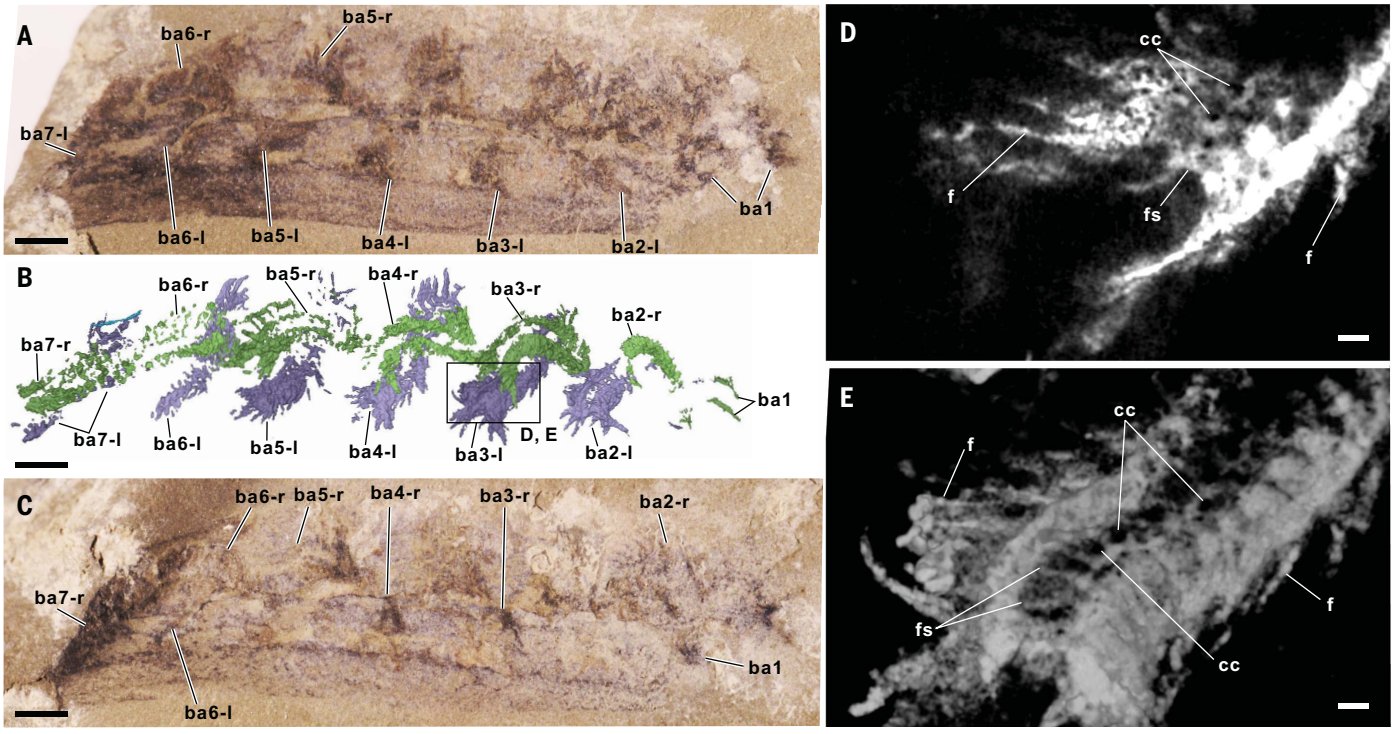

Fig. 2. X-ray computed microtomography of the branchial arches. (**A** to **C**) Photomicrographs of part (A) and mirrored counterpart (C) of specimen NIGP 176268 and its three-dimensional micro-CT reconstruction (B). (**D** and **E**) A selected slice and rendered image of the third left branchial arch show the cellular chambers. Abbreviations as in Fig. 1. Scale bars: 1 mm in (A) to (C), and 100 μm in (D) and (E).

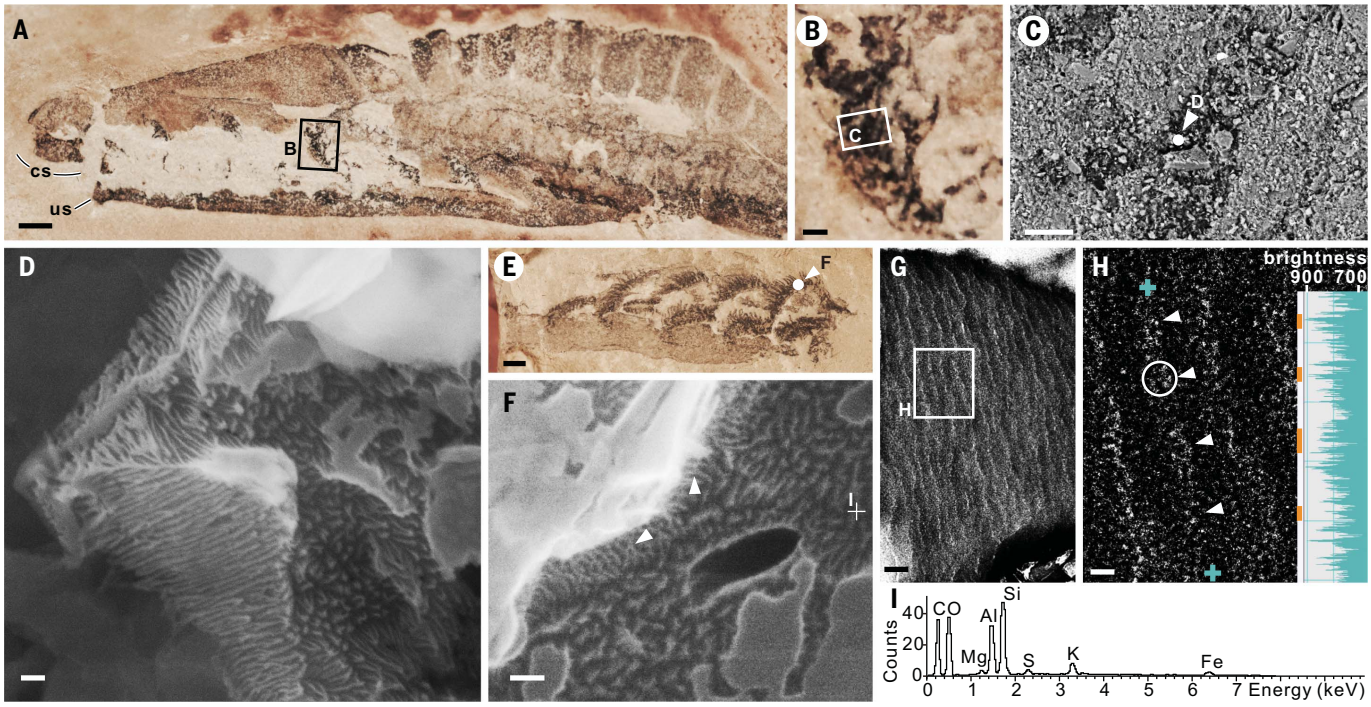

Fig. 3. Ultrastructure of the branchial arches of yunnanozoans. (**A**) An overview of the branchial arches of specimen NIGP 176258a. Abbreviations as in Fig. 1. (**B**) Enlarged view of the fifth arch [the boxed area in (A)]. (**C**) Backscattered scanning electron microscopy image of a straight septum [the boxed area in (B)]. (**D**) Secondary electron image shows that the carbon residues consist of bundles of microfibrils. (**E**) An overview of the branchial arches of specimen NIGP 176255. (**F**) Secondary electron image of the white point area in (E) shows the cross-linkages between the microfibrils (white arrowheads). (**G** and **H**) Transmission electron images show the microfibrils and the possible beads at 50-nm intervals (white arrowheads, one bead is circled) in specimen NIGP 176263. The inset in (H) is the brightness profile between the two cyan crosses, with positions of the possible beads marked by orange bars. (**I**) Energy dispersive spectrometry spectrum based on SEM at the white cross in (F). Scale bars: 1 mm in (A) and (E); 200 μm in (B); 50 μm in (C); 100 nm in (D), (F), and (G); and 20 nm in (H).

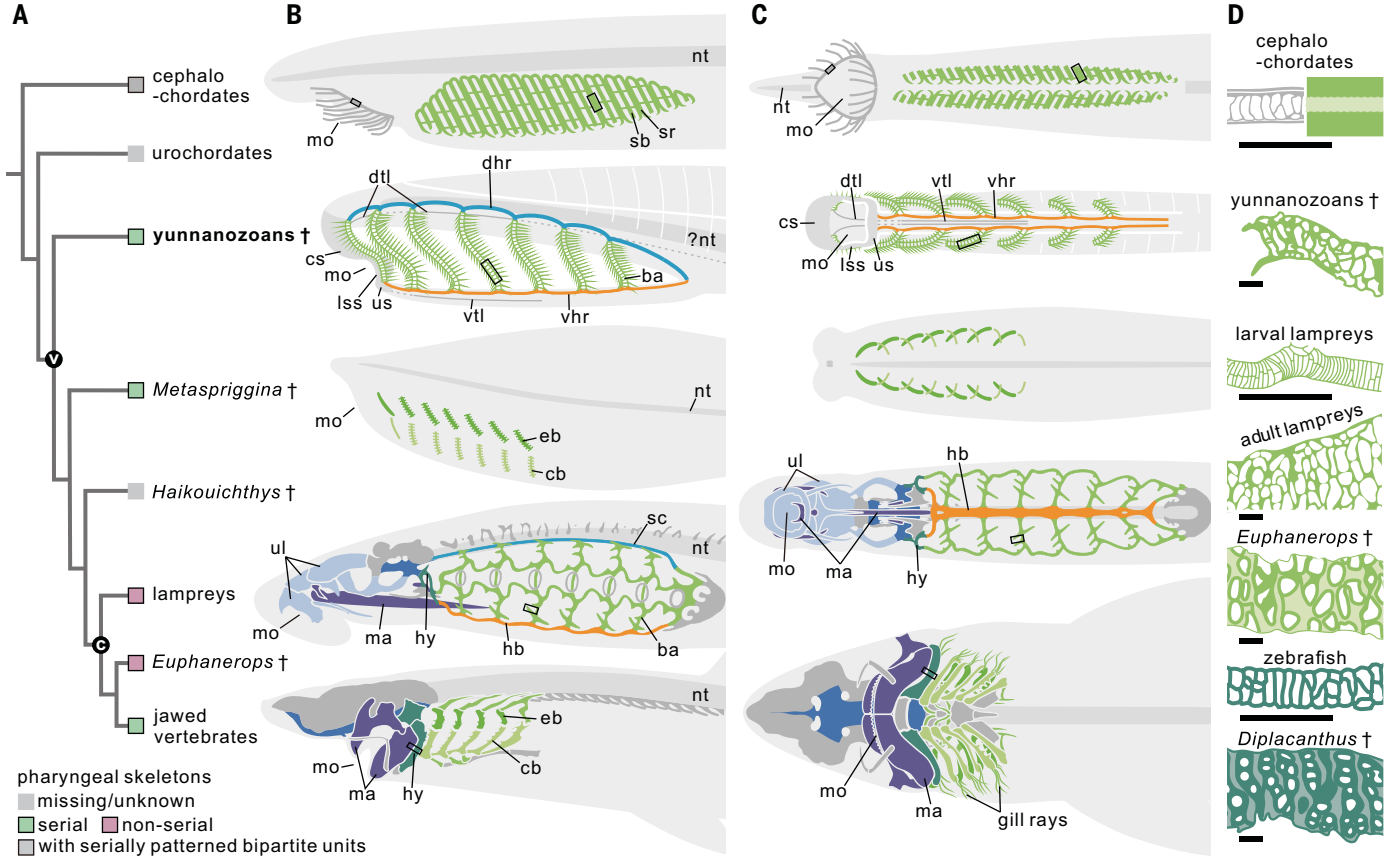

Fig. 4. Phylogenetic relationships and morphological comparisons of pharyngeal skeletons among representative clades of chordates. (**A**) Simplified consensus tree from Bayesian analyses (from fig. S6B), with morphological state of pharyngeal skeletons shown at the tips. This state is indicated as "serial" (green box), meaning the first arch resembles the other arches to form a series, or as "nonserial" (purple box), meaning the first arch has extensive skeleton and distinct from other arches. Cephalochordates are colored in gray, indicating that they have two alternate units of serially patterned arches. Encircled "V" indicates total-group vertebrates; encircled "C" means crown vertebrates. Fossil taxa are indicated with a single-dagger symbol. (**B** and **C**) Left and ventral views of the pharyngeal skeletons. (**D**) Chondrocyte arrangement in the boxed areas of the pharyngeal skeletons in (B) and (C). The left half in cephalochordates is from oral cirri, whereas the right half is from pharyngeal skeletons. Abbreviations: ba, branchial arches; cb, ceratobranchials; dhr/vhr, dorsal/ventral horizontal rod in yunnanozoans; dtl/vtl, dorsal/ventral thin horizontal line in yunnanozoans; eb, epibranchials; hb, hypobranchial bars in lamprey; hy, hyoid skeleton; ma, mandibular skeleton; nt, notochord; sc, subchordal bar in lamprey; sr/sb, skeleton in primary/secondary bar in cephalochordates; ul, upper lip cartilages in lamprey. For other abbreviations, see Fig. 1. Scale bars: 50 μm in (D). Images in (B) and (C) are not scaled. References and additional explanation of the drawings are available in supplementary text.

arch of the ancestral vertebrates was a typical branchial arch (*24*).

The yunnanozoan basket, with its successive, unjointed branchial arches that are connected by dorsal and ventral horizontal rods, is cyclostome-like (Fig. 4, B and C). Indeed, many researchers claim that the ancestral vertebrates had such an external basket (*3*) and not the deeper, jointed, and less interconnected arches seen in jawed fishes. This scenario, however, is challenged by the isolated and bipartite branchial bars in the higher stem vertebrates from the Cambrian, *Metaspriggina* and its relatives, the branchial skeletons of which are more gnathostome-like (Fig. 4) (*5*). This either implies that the cyclostome basket was secondarily derived and thus is merely convergent on the original, yunnanozoan basket—which is unlikely, given the real similarities we found here—or else it implies that *Metaspriggina* acquired a pre-gnathostome condition, having already lost the ancestral basket and gained the more separated arches.

REFERENCES AND NOTES

1. J. Mallatt, *J. Zool.* **204**, 169–183 (1984).
2. J. Mallatt, *Zoolog. Sci.* **25**, 990–998 (2008).
3. T. Miyashita, *Biol. Rev. Camb. Philos. Soc.* **91**, 611–657 (2016).
4. C. Hirschberger, V. A. Sleight, K. E. Criswell, S. J. Clark, J. A. Gillis, *Mol. Biol. Evol.* **38**, 4187–4204 (2021).
5. S. C. Morris, J.-B. Caron, *Nature* **512**, 419–422 (2014).
6. C. Yang, X.-H. Li, M. Zhu, D. J. Condon, J. Chen, *J. Geol. Soc. London* **175**, 659–666 (2018).
7. X. Hou, L. Ramskold, J. A. N. Bergstrom, *Zool. Scr.* **20**, 395–411 (1991).
8. J.-Y. Chen, J. Dzik, G. Edgecombe, L. Ramsköld, G. Q. Zhou, *Nature* **377**, 720–722 (1995).
9. D. Shu, X. Zhang, L. Chen, *Nature* **380**, 428–430 (1996).
10. J.-Y. Chen, D.-Y. Huang, C.-W. Li, *Nature* **402**, 518–522 (1999).
11. D. Shu *et al.*, *Science* **299**, 1380–1384 (2003).
12. J. Mallatt, J. Y. Chen, *J. Morphol.* **258**, 1–31 (2003).
13. P.-Y. Cong, X.-G. Hou, R. J. Aldridge, M. A. Purnell, Y. Z. Li, *Palaeontology* **58**, 45–70 (2015).
14. X. Hou, P. Cong, Y. Li, *Acta Palaeontol. Sin.* **48**, 402–413 (2009).
15. W. M. Martin, L. A. Bumm, D. W. McCauley, *Dev. Dyn.* **238**, 3126–3138 (2009).
16. C. B. Kimmel *et al.*, *Dev. Biol.* **203**, 245–263 (1998).
17. G. M. Wright, J. H. Youson, *Am. J. Anat.* **165**, 39–51 (1982).
18. G. M. Wright, F. W. Keeley, J. H. Youson, D. L. Babineau, *Am. J. Anat.* **169**, 407–424 (1984).
19. E. C. Davis, R. A. Roth, J. E. Heuser, R. P. Mecham, *J. Struct. Biol.* **139**, 65–75 (2002).
20. D. E. Birk, P. Brückner, in *The Extracellular Matrix: an Overview*, R. P Mecham, Ed. (Biology of Extracellular Matrix Series, Springer, Berlin Heidelberg, 2011), pp. 77–115.
21. G. M. Wright, F. W. Keeley, P. Robson, *Cell Tissue Res.* **304**, 165–174 (2001).
22. T. Miyashita, *Can. J. Zool.* **98**, 850–865 (2020).
23. P. Janvier, M. Arsenault, *Geodiversitas* **29**, 143–216 (2007).
24. G. De Beer, *The Development of the Vertebrate Skull* (Clarendon Press, 1937).

ACKNOWLEDGMENTS

We acknowledge M. Benton for comments and Z. Yang and Y. Wang for discussion. We also acknowledge the following individuals for their laboratory assistance: J. Tang, C. Wang, Y. Fang, and S. Wu at the Nanjing Institute of Geology and

Palaeontology, Chinese Academy of Sciences (NIGPAS); J. Chen, H. Liu, P. Jiang, and Z. Xia at the State Key Laboratory for Mineral Deposits Research, Nanjing University; G. Wang at Shanghai Jiao Tong University; and B. Wang, X. Lei, X. Chen, L. Hu, Z. Yin, R. Wu, T. Zhao, W. Zhang, and X. Zhao. We are grateful to two anonymous reviewers for their constructive comments and suggestions. **Funding:** Funding was provided by the Strategic Priority Research Program (B) of the Chinese Academy of Sciences [XDB26000000 (B.J., F.Z., and M.Z.)], the National Science Foundation of China [42288201 (B.J.); 41921002 and 42072006 (F.Z. and M.Z.)], and the Fundamental Research Funds for the Central Universities [0206-14380137 (B.J.)]. **Author contributions:** Conceptualization: F.Z. and B.J. Fossil collection: F.Z. and M.Z. Investigation: Q.T., F.Z., H.Z., and B.J. Funding acquisition: F.Z., M.Z., and B.J. Writing – original draft: Q.T., F.Z., and B.J. Writing – review & editing: Q.T., F.Z., H.Z., M.Z., and B.J. **Competing interests:** The authors declare that they have no competing interests. **Data and materials availability:** The specimens studied here are all stored in NIGPAS. The measurements and datasets for the phylogenetic analysis are available in the supplementary materials. Computed tomography data are deposited in MorphoSource at https://www.morphosource.org/projects/000378422?locale=en.

SUPPLEMENTARY MATERIALS

science.org/doi/10.1126/science.abm2708
Materials and Methods
Supplementary Text
Figs. S1 to S6
Tables S1 to S4
References (*25*–*64*)
MDAR Reproducibility Checklist
Data S1 to S3

Submitted 5 September 2021; accepted 17 May 2022
10.1126/science.abm2708

Science

Ultrastructure reveals ancestral vertebrate pharyngeal skeleton in yunnanozoans

Qingyi TianFangchen ZhaoHan ZengMaoyan ZhuBaoyu Jiang

Science, 377 (6602), • DOI: 10.1126/science.abm2708

Vertebrate ancestor?

Yunnanozoans are Cambrian animals with a taxonomic position that has long been debated with regard to whether they are ancestral chordates. Tian *et al*. use new imaging approaches on new yunnanozoan specimens and found evidence that their branchial arches are composed of cartilage within an extracellular matrix of micofibrils (see the Perspective by Miyashita). This combination of tissue types has been considered vertebrate specific, suggesting that this group of animals are indeed basal vertebrates. This relationship allows insight into the evolution of the pharyngeal skeleton (including the jaw and cranium) to be obtained from examination of this ancient progenitor. —SNV

Science (ISSN) is published by the American Association for the Advancement of Science. 1200 New York Avenue NW, Washington, DC 20005. The title *Science* is a registered trademark of AAAS.

Science
AAAS

Supplementary Materials for

Ultrastructure reveals ancestral vertebrate pharyngeal skeleton in yunnanozoans

Qingyi Tian *et al*.

Corresponding authors: Fangchen Zhao, fczhao@nigpas.ac.cn; Baoyu Jiang, byjiang@nju.edu.cn

Science **377**, 218 (2022)
DOI: 10.1126/science.abm2708

The PDF file includes:

Other Supplementary Material for this manuscript includes the following:

Materials and Methods

Provenance of the fossil specimens

All specimens involved in this study include the materials published in ref. *10* collected by J.Y. Chen and colleagues in 1999, and new materials collected by F.C. Zhao and M.Y. Zhu from 2016 to 2019. Those specimens were from the yellow mudstone of the Maotianshan Shale Member (518.0 ± 0.7 million years old) (*6*) of the Yu'anshan Formation in Haikou town, Kunming, China. The specimens are all housed in Nanjing Institute of Geology and Palaeontology, Chinese Academy of Sciences (NIGPAS) and can be accessed upon request (accession numbers in Data S1).

Photomicroscopy

Photographs of the fossils were taken with Carl Zeiss Axio Zoom V16 and Nikon D810. The photographs were optimized with Adobe Photoshop CC 2018 and CorelDRAW 2019 (Corel, Canada).

Measurements

Length and width of specific anatomical structures were measured on digital photographs. The body length of each specimen is measured by a curved line along the dorsal margin of the pharynx and gut. Lengths of the dorsal and ventral horizontal rods are represented by the distances between the attachment sites of the neighboring bamboo-like bars. All measurements are listed in Data S1.

X-ray computed microtomography

The specimens NIGP 176268 (the part and the counterpart; Fig. 2A, C) and NIGP 176264 (only the part; fig. S2G) were first scanned at Yinghua NDT, Shanghai, China using a GE phoenix v|tome|x M achieving voxel size of 11.3 and 9.11 μm, respectively. To achieve higher spatial resolution, NIGP 176268 was then scanned at the MicroCT Lab of NIGPAS using a three-dimensional X-ray microscope (3D-XRM), Zeiss Xradia 520 versa. Unlike conventional microCT which relies on maximum geometric magnification and flat-panel detector to obtain high resolution, 3D-XRM uses CCD-based objectives to get higher spatial resolution. Depending on the size of the specimen, a CCD-coupled 4× objective was employed, providing isotropic voxel size of 4.9 μm. The operating voltage for the X-ray tube was set to be 60 kV. During each scan, 2401 projections over 360° were obtained. To avoid artifacts of beam hardening, a thick X-ray filter (LE5) was used. Volume data processing, including three-dimensional volume renderings, 'ROI' (region of interest) segmentation, and virtual slicing, were performed using software VGstudio Max (3.0, Volume Graphics, Heidelberg, Germany) and Mimics v.20.0 (https://www.materialise.com/en/medical/mimics; Materialise, Leuven, Belgium). The data are deposited in MorphoSource at https://www.morphosource.org/projects/000378422?locale=en.

Scanning electron microscopy (SEM)

Specimens were observed under 15.00–25.00 kV with working distances of 10.0–13.3 mm, using a LEO 1530VP field-emission scanning electron microscope at the Technical Services Centre, NIGPAS. The modes of back-scattered electron, variable pressure secondary electron, and energy-dispersive X-ray spectroscopy were used.

Raman and Fourier-transform infrared (FTIR) spectroscopy

Raman and FTIR spectroscopy were applied to probe the chemical structure of the fossil. A sample was carefully removed from the filamentous arch of specimen NIGP 176263 using a dissecting scalpel (marked in fig. S3J). The sample was put into 0.05 mol/L hydrofluoric acid for 30 days to dissolve the sedimentary matrix and washed three times with distilled water. The acid-treated sample was dried on an aluminum foil for Raman spectroscopy analysis and on a CaF2 plate for FTIR spectroscopy analysis. The Raman spectrum was collected using a Horiba HR Evolution at the Technical Services Centre, NIGPAS (excitation wavelength 633 nm, 17 mW, 600 grooves/mm grating, 20s, 6 times). The infrared absorbance spectrum was collected using a Bruker Vertex 70V FTIR spectrometer coupled with a Hyperion 2000 microscope at the School of Earth Sciences and Engineering, Nanjing University (NJU) (60 × 60 μm aperture, 4 cm^{-1} resolution, 128 scans, KBr-Ge beam splitter, and Mercury-Cadmium-Telluride detector).

Transmission electron microscopy (TEM)

Part of the sample after FTIR spectroscopy analysis was embedded in Pon 812 resin (TED Pella, Inc.) and cut in ultrathin sections at the Instrumental Analysis Center, Shanghai Jiao Tong University. The sections were mounted on carbon-coated copper grids and observed under a FEI Tecnai G2 F20 S-TWIN TEM at 200kV at the School of Earth Sciences and Engineering, NJU. The TEM images were processed with Gatan Microscopy Suite (GMS) software (Fig. 3G, H).

Phylogenetic analysis

We examined the phylogenetic position of yunnanozoans in a newly combined dataset (Data S2). The dataset is a combination of the analysis of (*25*) including 37 major eukaryotic clades, two (*26, 27*) focusing on vetulicolians, and one (*28*) on early vertebrates. In the merged dataset, 59 repeated characters were removed (Table S1). The controversial fossil *Saccorhytus* was omitted (*26, 29, 30*). The character scores were based on (*31–34*).

To incorporate the controversial interpretations and our new results, we made some modifications to the merged dataset (Data S3). As for yunnanozoans, the controversial scores were all coded as '?' (Table S2). Some controversial scores of other taxa were also modified (Table S3). Based on our new observation, the states of six characters of yunnanozoans were corrected (Table S4), while four new characters were added (Supplementary Text).

Both the original merged dataset and the modified dataset (Data S2, S3) were analyzed in MrBayes v.3.2.7a (*35*) with default priors and Markov chain Monte Carlo (MCMC) settings. The analysis involved two independent runs of 50,000,000 MCMC generations, each containing four Markov chains under the Mkv + gamma model for discrete morphological character data (*36*). Tree samples were collected every 1,000 generations and with the first 25% of tree samples discarded as burn-in. The convergence of chains was checked by effective sample size (ESS) values over 3,200 and the 'fuzzy caterpillar'-shaped traces in Tracer v.1.7 (*37*) and was indicated by an average standard deviation of split frequencies below 0.01. The 50% majority-rule consensus trees of the original and the modified datasets are shown in fig. S6A and fig. S6B, respectively.

Supplementary Text

Description of the circumoral structure

The circumoral structure, interpreted as a big artery (*10, 12*), is composed of three continuous parts (Fig. 4B, C). First, dorsally, is a C-shaped, more horizontal part ('cs' in Fig. 1F;

fig. S1G–J, L, N). Second, laterally, is a pair of lobe-shaped structures that are more vertical and mildly curved concave-anterior ('lss' in Fig. 1H; fig. S1L–N; and it underlaps 'ba-1' in every figure that shows ba-1, including figs. S1E–J and S4C). The third part of the circumoral structure, ventrally, is a U-shaped structure on the mouth floor ('us' in Fig. 1H; fig. S1K–M). The first branchial arch is often fully or partly obscured by the underlapping circumoral structure in ventral views, especially by its lobe-shaped structures.

Measurements of the horizontal rods

The right and left horizontal rods are parallel and 0.3 ± 0.1 mm apart from each other (*N* = 34). They are 0.09 ± 0.04 mm in diameter (*N* = 21) and 1.7 ± 0.4 mm long (*N* = 121). The ventral horizontal rod length is in proportion to the body length (R^2 = 0.90, 32 rods on eight specimens) (Data S1). The rod length is used as a representation of the pharyngeal arch interval, whose relationship with body length contributes to a new character (character 315) for the phylogenetic analysis.

References and additional explanation of Fig. 4B–D

References of the left and ventral views of the pharyngeal skeletons in Fig. 4B–C: cephalochordate *Branchiostoma* (*38*, *39*); *Metaspriggina* (*5*); lamprey *Petromyzon* (*40*); shark *Squalus* (*41*).

In Fig. 4D, the diameters of the cellular chambers of yunnanozoans (23–84 μm) are consistent with chondrocytes of the counterpart cartilages in the adult sea lamprey *Petromyzon* (20–70 μm), the fossil, jawless anaspid fish *Euphanerops* (30–50 μm) and the stem-chondrichthyan "shark" *Diplacanthus* (20–60 μm), and are slightly larger than those of embryonic sea lamprey (ca. 20 μm) and zebrafish *Danio rerio* (ca. 15 μm). References of the chondrocyte arrangement: cephalochordates (*42*, *43*); larval lampreys (*15*); adult lampreys (*44*); *Euphanerops* (*23*); zebrafish (*16*); *Diplacanthus* (*45*).

Added characters and coding

Character 314. Pharyngeal endoskeleton. 0, acellular; 1, cellular. The pharyngeal cartilage is acellular in enteropneusts and cephalochordates (*42*). All living vertebrates have cellular cartilaginous or bony pharyngeal skeletons (*46*). The cellular cartilage has been described in the pharyngeal skeletons of the anapsid *Euphanerops* (*23*, *47*). The cellular bone in the jaws was previously reported in antiarchs (*48*) and arthrodires (*49*). This character is inapplicable to the taxa without gill bars (character 129).

Character 315. Pharyngeal slit growth versus body size. 0, negative allometry; 1, isometry or positive allometry. The growth pattern plots of different taxa are in Data S1.

Character 316. Stacked discoid arrangement of chondrocytes. 0, absent; 1, present; -, no chondrocytes. Cephalochordates have stacked chondrocytes in their oral cirri (Fig. 4D) (*43*). Some taxa in Arthropoda, Mollusca, and Annelida have stacked chondrocytes as well (*46*, *50*, *51*).

Character 317. Extracellular matrix composition of cartilages. 0, collagen-based; 1, noncollagen-based. Annelid *Sabella* (*50*), brachiopod *Terebratalia* (*52*), mollusk gastropods (*46*), mollusk *Sepia* and *Octopus* (*53*), and hemichordates (*54*) have collagens dominating their cartilage matrix. Arthropod *Limulus*, cephalochordates and cyclostomes have non-collagen dominated matrix filaments (*21*, *55*). The presence of collagen fiber bundles in *Birkenia*, *Rhyncholepis*, and Heterostraci is inferred from the morphology of the linear spaces (*56–58*).

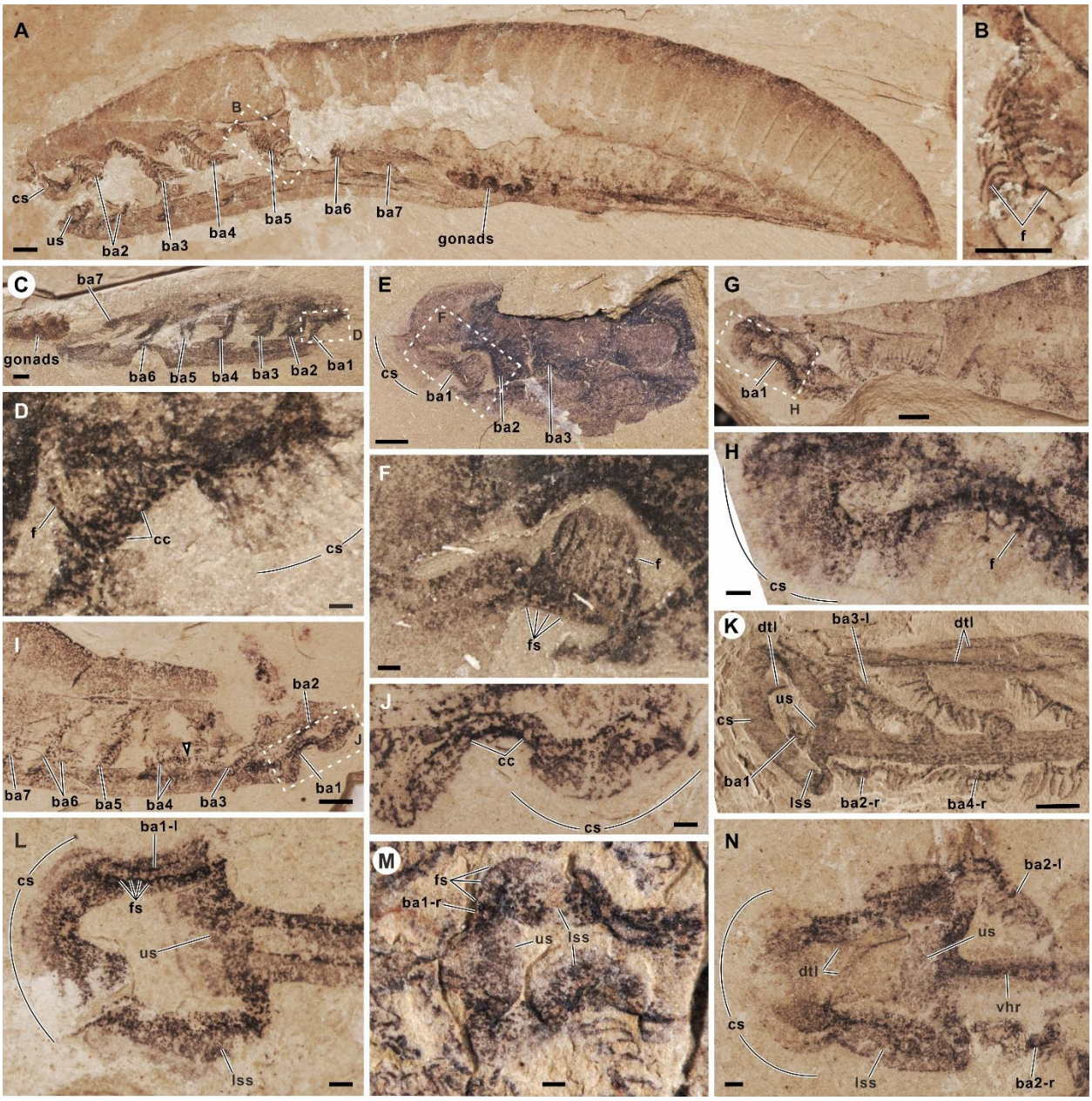

Fig. S1.

Additional photomicrographs show the detail of the branchial arches of yunnanozoans. (**A**–**B**) Enlarged view shows that each discoid structure corresponds to two filaments in the fifth arch in specimen NIGP 176257. (**C**–**H**) The laterally preserved first pair of arches with attached filaments. (C–D) NIGP176277; (E–F) NIGP 176269a; (G–H) EC00257a. (**I**–**J**) The bar of the first arch in the laterally preserved EC00041b. The arrowhead in (I) marks a disarticulated branchial arch. (**K**–**N**) Specimens in ventral view show the C-shaped, the lobe-shaped, and the U-shaped structures forming a circumoral structure. In L and N, rostral is to the left, but in M rostral is to the right. (K) EC00157; (L) EC00No02; (M) EC00308; (N) EC00333b. In (D), (F), (J), (L–M) first-order septa or cellular chambers are visible inside the bars of the first arches.

Abbreviations: dtl, dorsal thin horizontal line; vhr, ventral horizontal rod; the others are as in Fig. 1. Scale bars are 1 mm in A–C, E, G, I, K, 200 μm in D, F, H, J, L–N.

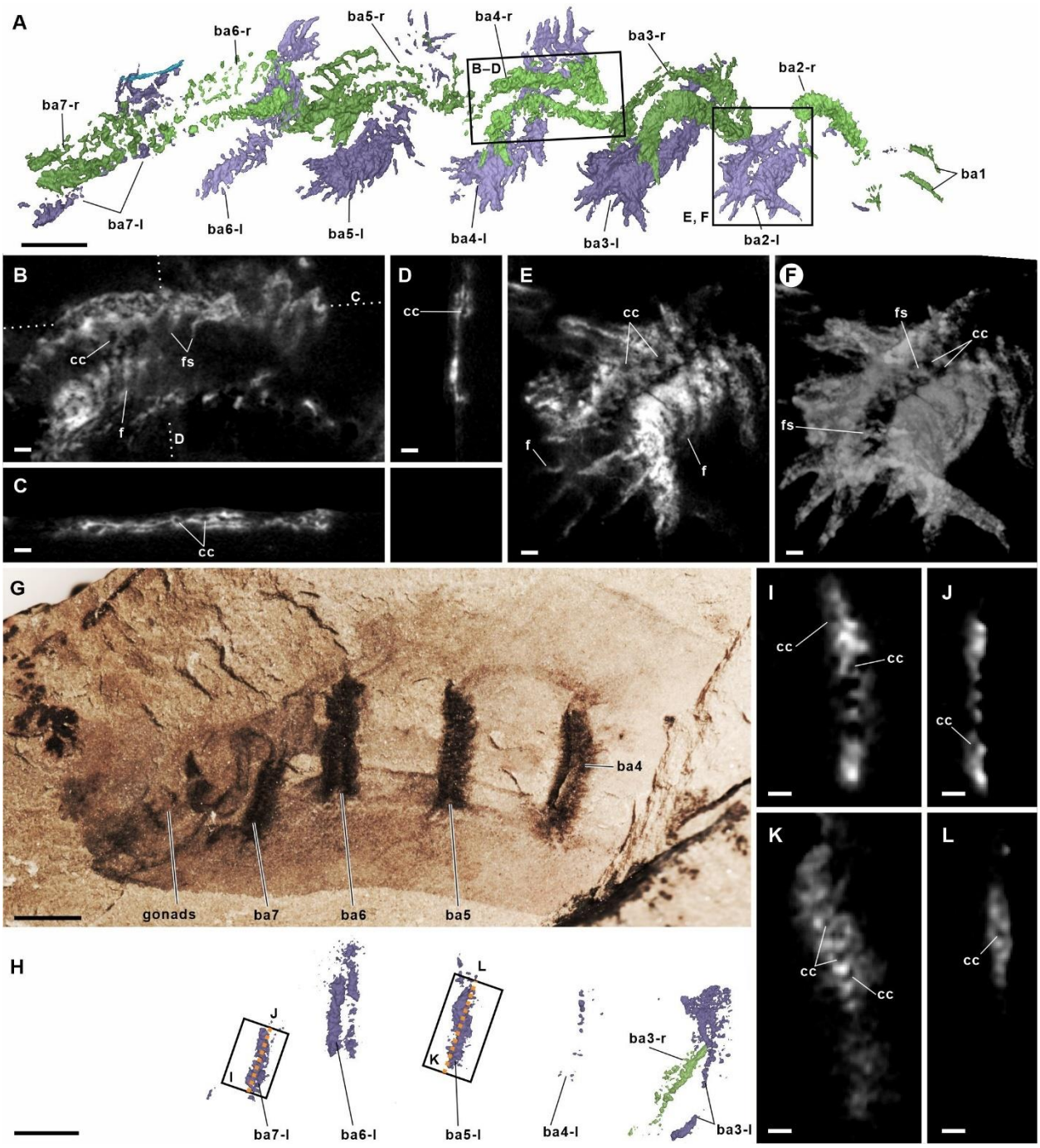

Fig. S2.

Additional X-ray computed microtomographs show the anatomy of the arches. (**A**) Three-dimensional anatomy of the seven pairs of arches in NIGP 176268. (**B**–**D**) Slices in three directions of the right fourth arch in NIGP 176268. The corresponding positions of the slices in (C) and (D) are marked by dotted lines in (B). (**E**–**F**) A selected slice and volume rendering of the left second arch in NIGP 176268. (**G**–**H**) Photomicrographs of specimen NIGP 176264 (G) and its three-dimensional anatomy (H). (**I**–**L**) Slices in two directions of the left seventh (I–J) and fifth arch (K–L) in NIGP 176264. The corresponding positions of the slices in (J) and (L) are

marked by orange dotted lines in (H). Abbreviations as in Fig. 1. Scale bars: 1 mm in A and G–H, 100 μm in B–F and I–L.

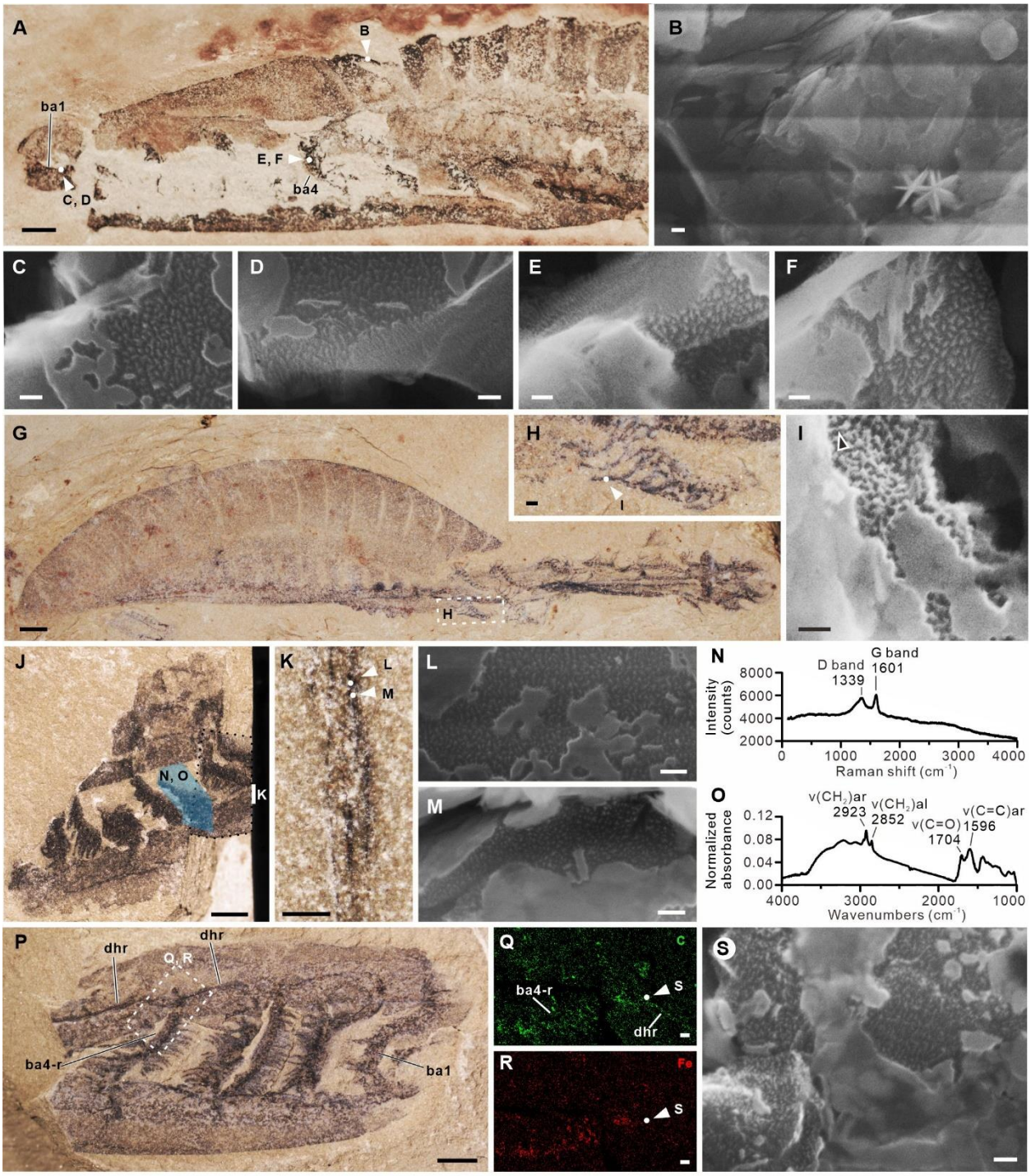

Fig. S3.

Additional data show the ultrastructure and chemical composition of the microfibrils. (**A**–**F**) SEM images (B–F) of specimen NIGP 176258a (A) show the microfibrils on the first (C, D) and the fifth branchial arches (E, F). (B) is an essential control image of the carbonaceous residue at the body margin, to show that the microfibrils only exist in branchial arches. Note in (D–E) the wavy arrangement of the microfibrils is visible on the vertical surfaces. (**G**–**I**) Photomicrographs (G–H) and SEM image (I) from a gill filament in specimen EC00213a (G)

show the microfibrils with extensive cross-linkages. One of the cross-linkages is marked by a black arrowhead. (**J**–**O**) Photomicrographs (J–K), SEM images (L–M), Raman (N) and FTIR (O) spectra from the specimen NIGP 176263. (K) is a section of the specimen, whose position is marked by the white bar in (J). Raman and FTIR spectra (N–O) were obtained from the hydrofluoric acid-treated materials in the blue shaded area in (J). The wavenumbers of the Raman shift and the FTIR peaks are shown, which are all consistent with the typical characteristic frequencies of carbonized materials (*59*, *60*). 'D band' and 'G band' are vibration signals of carbon lattice; 'ν' means stretching vibration signal of the chemical bond; 'ar' means aromatic bond; 'al' means aliphatic bond. (**P**–**S**) Photomicrograph (P), EDS elemental mapping of carbon (Q) and iron (R) of the dashed area in (P), and SEM image (S) from specimen NIGP 176267. Image S was taken on a dorsal horizontal rod shown in (Q–R). All SEM images were taken at the white points on the optic or EDS images. Abbreviations as in Figs. 1 and 4. Scale bar: 1 mm in A, G, J, and P; 100 μm in H, K, Q, and R; 100 nm in B–F, I, L–M, and S.

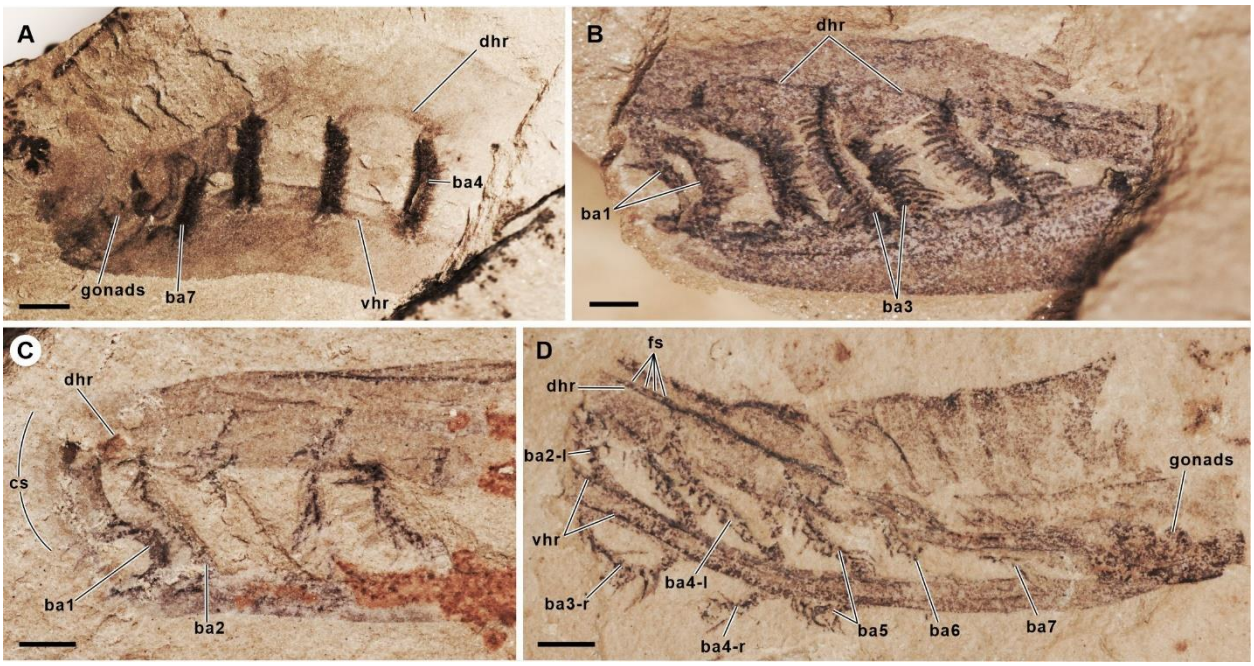

Fig. S4.

Additional photomicrographs show the dorsal horizontal rods. (**A**–**B**) Laterally preserved specimens with curved dorsal horizontal rod. (A) NIGP 176264; (B) NIGP 176267b; (**C**) Laterally preserved NIGP 176276 with dorsal horizontal rod linking the first and the second branchial arches. (**D**) Obliquely preserved NIGP 176274 with first-order septa inside the dorsal horizontal rod. Abbreviations: dhr, dorsal horizontal rod; vhr, ventral horizontal rod; the others see Fig. 1. Scale bars are all 1 mm.

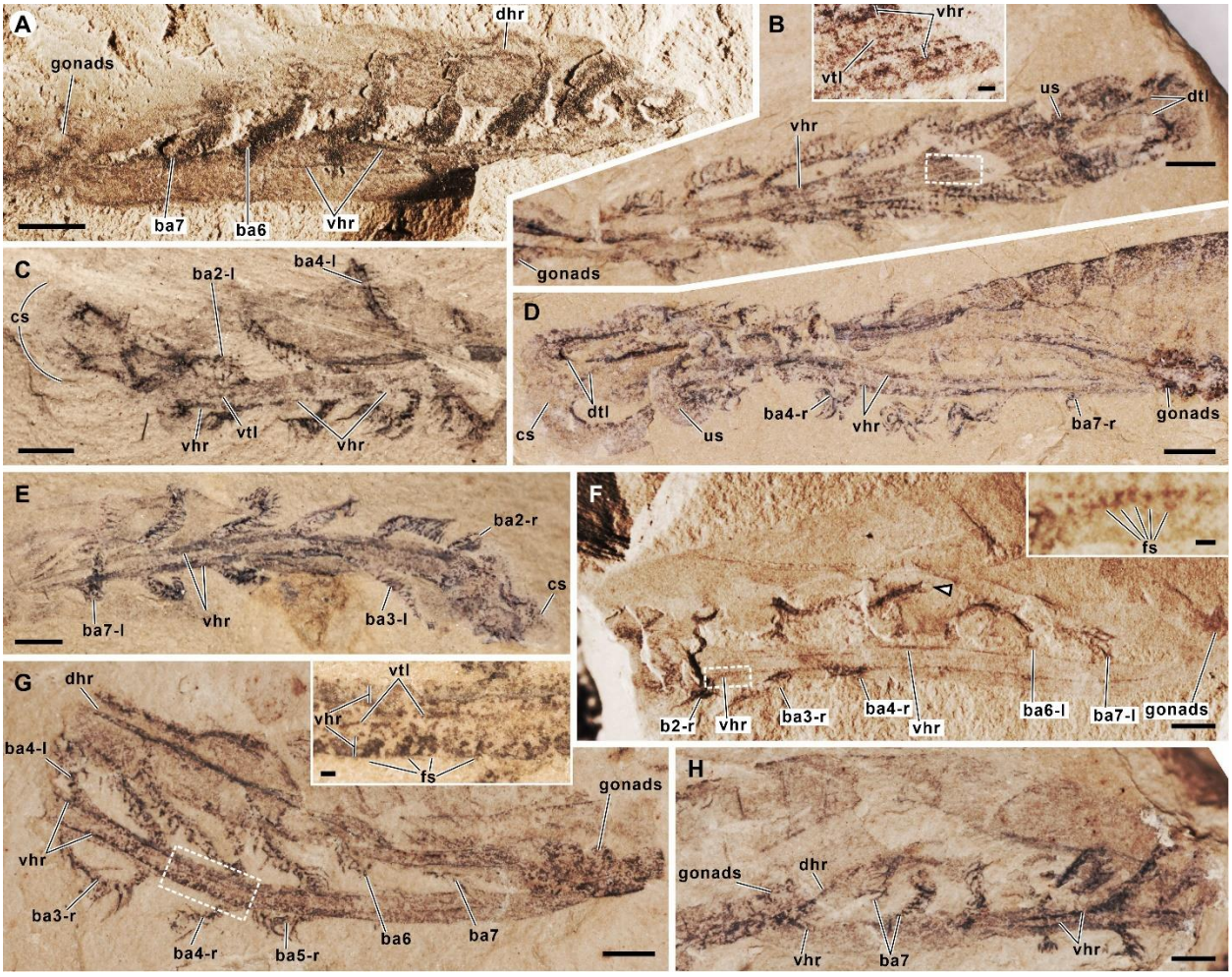

Fig. S5.

Additional photomicrographs show the ventral horizontal rods. (**A**) A laterally preserved specimen (NIGP 176262a) with curved ventral horizontal rods. (**B**–**C**) Ventrally exposed specimens (EC00231 and NIGP 176270) with curved ventral horizontal rods and ventral thin horizontal lines. (**D**–**E**) Paired ventral horizontal rods on ventrally exposed specimens. (D) EC00048a; (E) NIGP 176272; (**F**–**G**) First-order septa inside the ventral horizontal rods of EC00038a and NIGP 176274. The white arrowhead in (F) marks a disarticulated fifth branchial arch. (**H**) The dorsal and ventral horizontal rods converge toward each other in front of the gonads in specimen NIGP 176273. The inserts in (B) and (F–G) are the enlargements of the area in the dashed rectangles. Abbreviations see Figs. 1 and 4. Scale bars are 1 mm except being 100 μm in the inserts in B and F–G.

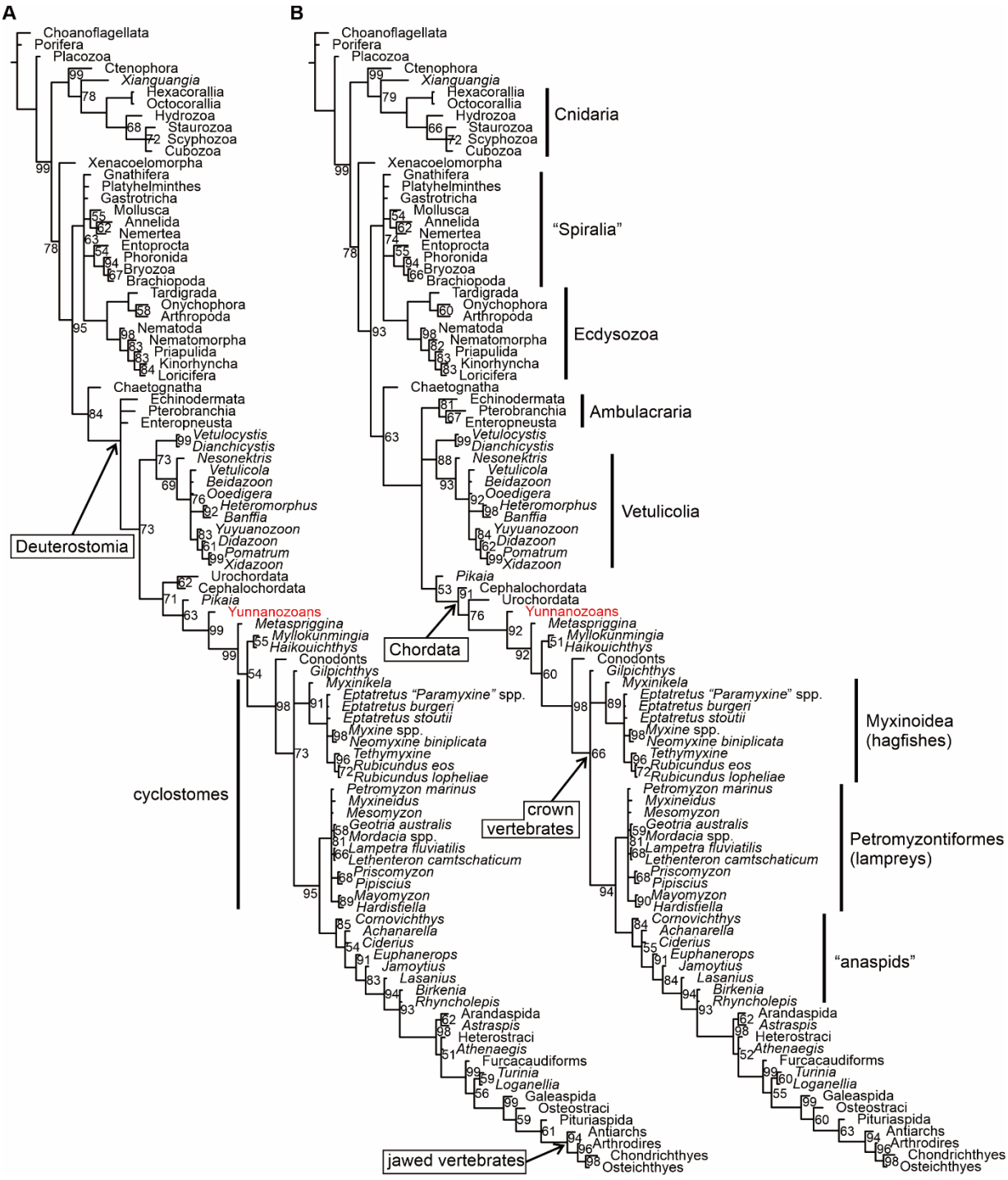

Fig. S6.

50% majority-rule consensus trees from Bayesian phylogenetic inference of metazoan relationships. (**A**) Consensus tree based on the unmodified merged matrix of 97 taxa and 313 characters. (**B**) Consensus tree based on the modified merged matrix of 97 taxa and 317 characters. Nodal supports are posterior probabilities, and those of the numberless nodes are 100%. 'Modified' means certain characters were adjusted, according to Tables S2–S4. Major taxonomic groups are indicated by bars and labels beside the tips.

Table S1.

Repeated characters in the merged dataset. Characters in the same row are repeated. The most recent characters are retained and the earlier ones are removed.

Character	In (*28*)	In (*25*)	In (*26*)	In (*27*)
#8 Epithelia		#8	#25	
#13 Diffuse nervous system		#13	#33	
#21Body symmetry		#21	#3	
#46 Circular depression on basal disc		#46	#37	
#67 Through-gut		#67	#14	
#69 Protonephridia (or homologues)		#69	#7	
#70 Fate of blastopore		#70	#2	
#71 Body cuticle with chitin		#71	#26	#6
#72 Body cuticel with α-chitin		#72	#27	
#73 Body cuticle molted		#73	#28	
#80 Teloblastic segmentation		#80	#18	
#81 Longitudinal ventral nerve cord(s)		#81	#34	
#82 Circum-pharyngeal, collar-shaped brain with anterior and posterior rings of perikarya separated by a ring-shaped neuropil		#82	#31	
#83 Introvert with scalid rings		#83	#12	
#85 Immunoreactivity of horseradish peroxidase (HRP)		#85	#61	
#88 Circum-oral, radially-arranged tentacles		#88		#26
#90 Trochophores		#90	#55	
#98 Coelom formation		#98	#4, #5	
#99 Trimeric coelom		#99	#6	
#100 Pharyngeal slits		#100		#22
#101 Endostyle (or homologues)		#101	#45	
#102 Notochord		#102	#48	#12
#106 Tornaria-type larva		#106	#54	
#107 Longitudinal dorsal nerve cord		#107	#35	#14
#307 Inflected myomeres	#161	#108	#51	#3, #4, #5
#147 Skeletal derivatives of neural crest	#1	#110	#52	
#148 Ectodermal placodes	#2	#111	#53	
#20 Spiral cleavage with 4d mesoderm; #97 Radial cleavage		#20, #97	#1	
#109 Body division			#8	#1
#113 Segmentation or metamerism			#16	#2
#309 Anus, with respect to distribution of mesoderm	#163		#15	#11
#209 Position of mouth	#63		#9	#16
#128 Gill bars/arches			#42	#19
#197 Respiratory current exits through	#51		#47	#23
#130 Filter feeding accomplished within pharynx			#44	#24
#110 Mouth surrounded by oral folds or plates; #111 Multi-circlets of oral folds			#10, #11	#29
#123 Longitudinal lateral grooves (median zone).			#36	#30
#117 Shape of anterior body region			#21	#31
#124 Body cones			#38	#33
#193 Pharyngeal skeleton	#47			#20
#200–203 Number of arches (or pouches) in branchial apparatus	#55, #56, #57			#21
#226 Body forms, width against height	#80			#7, #8
#227 Endoskeletal fin supports	#81			#10
#228 Distinct dorsal fin; #231 Distinct anal fin; #234 Preanal skin fold (epidermal ridge)	#82, #85, #88			#9
#121 Three-layered cuticle			#29 repeated with #30	

Table S2.

Controversial scores of yunnanozoans.

Character	In (*28*)	In (*25*)	In (*26*)	In (*27*)	In (*61*)	In (*61*) according to (*62*)	In (*56*)	In (*12*)	After modification
#71 Body cuticle. 0, absent; 1, present		#71		#6, '0'	#6, '0'	#6, '1'			→'?'
#107 Longitudinal dorsal nerve cord. 0, absent; 1, present		#107		#14, '1'	#14, '1'	#14, '0'			→'?'
#110 Body division. 0, uniparitite body; 1, bipartite; 2, tripartite			#8	#1, '0'	#1, '0'	#1, '1-distinct anterior and posterior body present'			→'0/1'
#102 Notochord. 0, absent; 1, present		#102		#12, '1'	#12, '1'	#12, '0'			→'?'
#144 Notochord extension. 0, extends along most of body; 1, restricted to posterior region of body				#27, '0-extends along most of body'					→'?'
#148 Ectodermal placode. 0, absent; 1, present	#2, '1'								→'?'
#172 Eye with retinal pigmented epithelium. 0, absent; 1, present; #174 Eyes. 0, exposed; 1, covered by dermis; 2, covered by trunk muscles; #179 Eyes. 0, laterally placed (interorbital distance equal to width of head at that position); 1, close together near midline (interorbital distance substantially less than width of head at that position); 2, on prominent eyestalk	#26, '1'; #27, '0'; #32, '0'			#13 paired eyes, '?'	#13 paired eyes, '1'	#13 paired eyes, '0'			→'?', '?', '?'
#228 Distinct dorsal fin. 0, absent; 1, present	#82, '0'							#30 dorsal fin, '1'	→'?'
#234 Preanal skin fold (epidermal ridge). 0, absent; 1, present; #236 Preanal skin fold (epidermal ridge). 0, absent; 1, present; #237 Preanal skin fold (epidermal ridge). 0, longitudinal; 1, discrete pelvic fins	#88, '1-present'; #89, '0-midline'; #90, '0-longitudinal'						#39, preanal median fold, '0-absent'		→'?', '?', '?'
#307 Inflected myomeres. 0, Z-shaped; 1, W-shaped	#161, '0, Z-shaped'			#4 myomeres, 'present'	#4 myomeres, 'present'	#4 myomeres, 'absent'		#36, myomeres, 'straight'	→'?'
#309 Anus, with respect to distribution of mesoderm. 0, terminal or subterminal; 1, non-terminal	#163, '0, terminal or subterminal'			#11 '1-post-anal tail (sub-terminal anus)'	#11 '-post-anal tail'	#11 terminal anus (0) versus post-anal tail (1), '?'		#32 '1, post-anal tail'	→'?'

Table S3.

Controversial scores of other taxa.

Taxon	Character	In (*25*)	In (*26*)	In (*27*)	In (*61*)	In (*61*) according to (*62*)	Note and reference	After modification
Echinodermata	#142 Wide pharyngeal cavity or wide anterior foregut. 0, absent; 1, present			#18, '0'			Basal Echinodermata fossils were interpreted having pharyngeal basket feeders (*63*)	→'0/1'
	#130 Filter feeding accomplished within pharynx. 0, absent; 1, present		#44, '0'					→'0/1'
	#131 Pharyngeal food-transport groove. 0, absent; 1, present		#46, '-'					→'?'
	#128 Gill bars/arches. 0, absent; 1, present		#42, '-'					→'?'
	#129 Gill cowls (hoods). 0, absent; 1, present		#43, '-'					→'0'
	#141 Buccal cavity. 0, absent; 1, present			#17, '-'			(*64*)	→'0/1'
Vetulicola, *Beidazoon*, *Ooedigera*, *Pomatrum*, *Xidazoon*, *Didazoon*, *Yuyuanozoon*, *Heteromorphus*, *Banffia*, *Vetulocystis*, *Dianchicystis*	#128 Gill bars/arches. 0, absent; 1, present		#44, '0-absent'	#19, '?'	#19, '?'		We chose the more conservative score	→'?'
Nesonektris	#102 Notochord. 0, absent, 1, present	#102, '1'					The notochord of *Nesonektris* is controversial	→'?'
	#144 Notochord extension. 0, extends along most of body; 1, restricted to posterior region of body			#27, '1'				→'?'
	#145 Notochord type. 0, "stack of coins", 1, vacuolar and longitudinally continuous.			#28, '0'				→'?'
Pikaia	#130 Filter feeding accomplished within pharynx. 0, absent; 1, present		#44	'0-no suspension feeder'	'0-no suspension feeder'	'1-bona fide suspension feeder'.	The feeding method of *Pikaia* is controversial	→'?'
Cephalochordata	#109 Body division. 0, uniparitite body; 1, bipartite; 2, tripartite		#8, '1'				The body division of Cephalochordata is similar to that of vertebrates	→'0'

Table S4.

Score modification based on the new observation of yunnanozoans.

Characters	In (*28*)	Explanation	After modification
#147 Skeletal derivatives of neural crest. 0, absent; 1, present	#1, '0'		→'?'
#194 Main skeletal support for branchial apparatus with respect to lamellae. 0, lateral; 1, medial	#48, '-'	(Fig. 1H; fig. S5B, D, G)	→'1'
#195 Pharyngeal skeleton. 0, skeletal arches fused with each other; 1, arches isolated	#49, '?'		→'0'
#210 Epidermal oral cirri. 0, absent; 1, present	#64, '1'	The filaments on the first arches are similar to those on the posterior arches	→'0'
#245 Cellular cartilages with hypertrophied chondrocytes (30-50 μm in diameter). 0, absent; 1, present	#99, '?'	The interpreted chondrocytes in yunnanozoans are in this size	→'1'
#246 Mature chondrocytes. 0, become separated and generally even spaced by extracellular matrix; 1, remain nested in a pair	#100, '?'		→'0'

References and Notes

1. J. Mallatt, Early vertebrate evolution: Pharyngeal structure and the origin of gnathostomes. *J. Zool.* **204**, 169–183 (1984). doi:10.1111/j.1469-7998.1984.tb02368.x

2. J. Mallatt, The origin of the vertebrate jaw: Neoclassical ideas versus newer, development-based ideas. *Zoolog. Sci.* **25**, 990–998 (2008). doi:10.2108/zsj.25.990 Medline

3. T. Miyashita, Fishing for jaws in early vertebrate evolution: A new hypothesis of mandibular confinement. *Biol. Rev. Camb. Philos. Soc.* **91**, 611–657 (2016). doi:10.1111/brv.12187 Medline

4. C. Hirschberger, V. A. Sleight, K. E. Criswell, S. J. Clark, J. A. Gillis, Conserved and unique transcriptional features of pharyngeal arches in the skate (*Leucoraja erinacea*) and evolution of the jaw. *Mol. Biol. Evol.* **38**, 4187–4204 (2021). doi:10.1093/molbev/msab123 Medline

5. S. C. Morris, J.-B. Caron, A primitive fish from the Cambrian of North America. *Nature* **512**, 419–422 (2014). doi:10.1038/nature13414 Medline

6. C. Yang, X.-H. Li, M. Zhu, D. J. Condon, J. Chen, Geochronological constraint on the Cambrian Chengjiang biota, South China. *J. Geol. Soc. London* **175**, 659–666 (2018). doi:10.1144/jgs2017-103

7. X. Hou, L. Ramskold, J. A. N. Bergstrom, Composition and preservation of the Chengjiang fauna — A Lower Cambrian soft-bodied biota. *Zool. Scr.* **20**, 395–411 (1991). doi:10.1111/j.1463-6409.1991.tb00303.x

8. J.-Y. Chen, J. Dzik, G. Edgecombe, L. Ramsköld, G. Q. Zhou, A possible Early Cambrian chordate. *Nature* **377**, 720–722 (1995). doi:10.1038/377720a0

9. D. Shu, X. Zhang, L. Chen, Reinterpretation of *Yunnanozoon* as the earliest known hemichordate. *Nature* **380**, 428–430 (1996). doi:10.1038/380428a0

10. J.-Y. Chen, D.-Y. Huang, C.-W. Li, An early Cambrian craniate-like chordate. *Nature* **402**, 518–522 (1999). doi:10.1038/990080

11. D. Shu, S. C. Morris, Z. F. Zhang, J. N. Liu, J. Han, L. Chen, X. L. Zhang, K. Yasui, Y. Li, A new species of yunnanozoan with implications for deuterostome evolution. *Science* **299**, 1380–1384 (2003). doi:10.1126/science.1079846 Medline

12. J. Mallatt, J. Y. Chen, Fossil sister group of craniates: Predicted and found. *J. Morphol.* **258**, 1–31 (2003). doi:10.1002/jmor.10081 Medline

13. P.-Y. Cong, X.-G. Hou, R. J. Aldridge, M. A. Purnell, Y. Z. Li, New data on the palaeobiology of the enigmatic yunnanozoans from the Chengjiang Biota, Lower Cambrian, China. *Palaeontology* **58**, 45–70 (2015). doi:10.1111/pala.12117

14. X. Hou, P. Cong, Y. Li, On the taphonomy and phylogenetic relationships of yunnanozoans (in Chinese with English summary). *Acta Palaeontol. Sin.* **48**, 402–413 (2009).

15. W. M. Martin, L. A. Bumm, D. W. McCauley, Development of the viscerocranial skeleton during embryogenesis of the sea lamprey, *Petromyzon Marinus*. *Dev. Dyn.* **238**, 3126–3138 (2009). doi:10.1002/dvdy.22164 Medline

16. C. B. Kimmel, C. T. Miller, G. Kruze, B. Ullmann, R. A. BreMiller, K. D. Larison, H. C. Snyder, The shaping of pharyngeal cartilages during early development of the zebrafish. *Dev. Biol.* **203**, 245–263 (1998). doi:10.1006/dbio.1998.9016 Medline

17. G. M. Wright, J. H. Youson, Ultrastructure of mucocartilage in the larval anadromous sea lamprey, *Petromyzon marinus* L. *Am. J. Anat.* **165**, 39–51 (1982). doi:10.1002/aja.1001650105 Medline

18. G. M. Wright, F. W. Keeley, J. H. Youson, D. L. Babineau, Cartilage in the Atlantic hagfish, *Myxine glutinosa*. *Am. J. Anat.* **169**, 407–424 (1984). doi:10.1002/aja.1001690404 Medline

19. E. C. Davis, R. A. Roth, J. E. Heuser, R. P. Mecham, Ultrastructural properties of ciliary zonule microfibrils. *J. Struct. Biol.* **139**, 65–75 (2002). doi:10.1016/S1047-8477(02)00559-2 Medline

20. D. E. Birk, P. Brückner, "Collagens, suprastructures, and collagen fibril assembly" in *The Extracellular Matrix: an Overview*, R. P Mecham, Ed. (Biology of Extracellular Matrix Series, Springer, Berlin Heidelberg, 2011), pp. 77–115.

21. G. M. Wright, F. W. Keeley, P. Robson, The unusual cartilaginous tissues of jawless craniates, cephalochordates and invertebrates. *Cell Tissue Res.* **304**, 165–174 (2001). doi:10.1007/s004410100374 Medline

22. T. Miyashita, A Paleozoic stem hagfish *Myxinikela siroka* — revised anatomy and implications for evolution of the living jawless vertebrate lineages. *Can. J. Zool.* **98**, 850–865 (2020). doi:10.1139/cjz-2020-0046

23. P. Janvier, M. Arsenault, The anatomy of *Euphanerops longaevus* Woodward, 1900, an anaspid-like jawless vertebrate from the Upper Devonian of Miguasha, Quebec, Canada. *Geodiversitas* **29**, 143–216 (2007).

24. G. De Beer, *The Development of the Vertebrate Skull* (Clarendon Press, 1937).

25. Q. Ou, J. Han, Z. Zhang, D. Shu, G. Sun, G. Mayer, Three Cambrian fossils assembled into an extinct body plan of cnidarian affinity. *Proc. Natl. Acad. Sci. U.S.A.* **114**, 8835–8840 (2017). doi:10.1073/pnas.1701650114 Medline

26. J. Han, S. C. Morris, Q. Ou, D. Shu, H. Huang, Meiofaunal deuterostomes from the basal Cambrian of Shaanxi (China). *Nature* **542**, 228–231 (2017). doi:10.1038/nature21072 Medline

27. D. C. García-Bellido, M. S. Y. Lee, G. D. Edgecombe, J. B. Jago, J. G. Gehling, J. R. Paterson, A new vetulicolian from Australia and its bearing on the chordate affinities of an enigmatic Cambrian group. *BMC Evol. Biol.* **14**, 214 (2014). doi:10.1186/s12862-014-0214-z Medline

28. T. Miyashita, R. W. Gess, K. Tietjen, M. I. Coates, Non-ammocoete larvae of Palaeozoic stem lampreys. *Nature* **591**, 408–412 (2021). doi:10.1038/s41586-021-03305-9 Medline

29. D. Shu, J. Han, Core value of the Chengjiang fauna: Formation of the animal kingdom and the birth of basic human organs (English). *Earth Sci. Front* **27**, 382–412 (2020).

30. Y. Liu, H. Zhang, S. Xiao, T. Shao, B. Duan, An early Cambrian ecdysozoan with a terminal mouth but no anus. bioRxiv 2020.09.04.283960 [Preprint] (2020). https://doi.org/10.1101/2020.09.04.283960.

31. A. Schmidt-Rhaesa, *The Evolution of Organ Systems* (Oxford Univ. Press, 2007).

32. E. M. Costa-Paiva, C. G. Schrago, K. M. Halanych, Broad phylogenetic occurrence of the oxygen-binding hemerythrins in bilaterians. *Genome Biol. Evol.* **9**, 2580–2591 (2017). doi:10.1093/gbe/evx181 Medline

33. J. M. Martín-Durán, A. Hejnol, A developmental perspective on the evolution of the nervous system. *Dev. Biol.* **475**, 181–192 (2021). doi:10.1016/j.ydbio.2019.10.003 Medline

34. K. J. Peterson, D. J. Eernisse, Animal phylogeny and the ancestry of bilaterians: Inferences from morphology and 18S rDNA gene sequences. *Evol. Dev.* **3**, 170–205 (2001). doi:10.1046/j.1525-142x.2001.003003170.x Medline

35. F. Ronquist, M. Teslenko, P. van der Mark, D. L. Ayres, A. Darling, S. Höhna, B. Larget, L. Liu, M. A. Suchard, J. P. Huelsenbeck, MrBayes 3.2: Efficient Bayesian phylogenetic inference and model choice across a large model space. *Syst. Biol.* **61**, 539–542 (2012). doi:10.1093/sysbio/sys029 Medline

36. P. O. Lewis, A likelihood approach to estimating phylogeny from discrete morphological character data. *Syst. Biol.* **50**, 913–925 (2001). doi:10.1080/106351501753462876 Medline

37. A. Rambaut, A. J. Drummond, D. Xie, G. Baele, M. A. Suchard, Posterior summarization in Bayesian phylogenetics using Tracer 1.7. *Syst. Biol.* **67**, 901–904 (2018). doi:10.1093/sysbio/syy032 Medline

38. M. Urata, N. Yamaguchi, Y. Henmi, K. Yasui, Larval development of the oriental lancelet, *Branchiostoma belcheri*, in laboratory mass culture. *Zoolog. Sci.* **24**, 787–797 (2007). doi:10.2108/zsj.24.787 Medline

39. J. Müller, *Über den Bau und die Lebenserscheinungen des Branchiostoma lubricum Costa, Amphioxus lanceolatus Yarrel* (Dümmler, Berlin, 1844).

40. W. Marinelli, A. Strenger, *Vergleichende Anatomie und Morphologie der Wirbeltiere. I Lieferung. Lampetra fluviatilis (L)* (Deuticke, Wien, 1954).

41. W. F. Walker, *Vertebrate Dissection* (Saunders, ed. 6, 1980).

42. A. L. Rychel, B. J. Swalla, Development and evolution of chordate cartilage. *J. Exp. Zool. B Mol. Dev. Evol.* **308**, 325–335 (2007). doi:10.1002/jez.b.21157 Medline

43. D. Jandzik, A. T. Garnett, T. A. Square, M. V. Cattell, J.-K. Yu, D. M. Medeiros, Evolution of the new vertebrate head by co-option of an ancient chordate skeletal tissue. *Nature* **518**, 534–537 (2015). doi:10.1038/nature14000 Medline

44. P. Robson, G. M. Wright, J. H. Youson, F. W. Keeley, A family of non-collagen-based cartilages in the skeleton of the sea lamprey, *Petromyzon marinus*. *Comp. Biochem. Physiol. B Biochem. Mol. Biol.* **118**, 71–78 (1997). doi:10.1016/S0305-0491(97)00026-6

45. M. D. Brazeau, S. Giles, R. P. Dearden, A. Jerve, Y. Ariunchimeg, E. Zorig, R. Sansom, T. Guillerme, M. Castiello, Endochondral bone in an Early Devonian ‘placoderm’ from

Mongolia. *Nat. Ecol. Evol.* **4**, 1477–1484 (2020). doi:10.1038/s41559-020-01290-2 Medline

46. B. K. Hall, *Bones and Cartilage* (Elsevier, 2015).

47. P. Janvier, M. Arsenault, Palaeobiology: Calcification of early vertebrate cartilage. *Nature* **417**, 609–609 (2002). doi:10.1038/417609a Medline

48. Z. Johanson, Placoderm branchial and hypobranchial muscles and origins in jawed vertebrates. *J. Vertebr. Paleontol.* **23**, 735–749 (2003). doi:10.1671/2

49. M. Rücklin, P. C. J. Donoghue, Z. Johanson, K. Trinajstic, F. Marone, M. Stampanoni, Development of teeth and jaws in the earliest jawed vertebrates. *Nature* **491**, 748–751 (2012). doi:10.1038/nature11555 Medline

50. H. Kryvi, The fine structure of the cartilage in the annelid *Sabella penicillum*. *Protoplasma* **91**, 191–200 (1977). doi:10.1007/BF01276733 Medline

51. R. D. Farley, Ultrastructure of book gill development in embryos and first instars of the horseshoe crab *Limulus polyphemus* L. (Chelicerata, Xiphosura). *Front. Zool.* **9**, 4 (2012). doi:10.1186/1742-9994-9-4 Medline

52. S. A. Stricker, C. G. Reed, Development of the pedicle in the articulate brachiopod *Terebratalia transversa* (Brachiopoda, Terebratulida). *Zoomorphology* **105**, 253–264 (1985). doi:10.1007/BF00311968

53. A. Bairati, S. De Biasi, F. Cheli, A. Oggioni, The head cartilage of cephalopods. I. Architecture and ultrastructure of the extracellular matrix. *Tissue Cell* **19**, 673–685 (1987). doi:10.1016/0040-8166(87)90074-7 Medline

54. F. Pardos, J. Benito, Blood vessels and related structures in the gill bars of *Glossobalanus minutus* (Enteropneusta). *Acta Zool.* **69**, 87–94 (1988). doi:10.1111/j.1463-6395.1988.tb00905.x

55. P. Person, D. E. Philpott, The biology of cartilage. I. Invertebrate cartilages: *Limulus* gill cartilage. *J. Morphol.* **128**, 67–93 (1969). doi:10.1002/jmor.1051280104

56. S. Turner, C. J. Burrow, H.-P. Schultze, A. Blieck, W.-E. Reif, C. B. Rexroad, P. Bultynck, G. S. Nowlan, False teeth: Conodont-vertebrate phylogenetic relationships revisited. *Geodiversitas* **32**, 545–594 (2010). doi:10.5252/g2010n4a1

57. J. N. Keating, P. C. J. Donoghue, Histology and affinity of anaspids, and the early evolution of the vertebrate dermal skeleton. *Proc. Biol. Sci.* **283**, 20152917 (2016). doi:10.1098/rspb.2015.2917 Medline

58. J. N. Keating, C. L. Marquart, F. Marone, P. C. J. Donoghue, The nature of aspidin and the evolutionary origin of bone. *Nat. Ecol. Evol.* **2**, 1501–1506 (2018). doi:10.1038/s41559-018-0624-1 Medline

59. A. Schito, C. Romano, S. Corrado, D. Grigo, B. Poe, Diagenetic thermal evolution of organic matter by Raman spectroscopy. *Org. Geochem.* **106**, 57–67 (2017). doi:10.1016/j.orggeochem.2016.12.006

60. P. Painter, M. Starsinic, M. Coleman, “Determination of functional groups in coal by Fourier transform interferometry” in *Fourier Transform Infrared Spectra* (Elsevier, 1985), vol. 4, pp. 169–241.

61. J. Mallatt, N. Holland, *Pikaia gracilens* Walcott: Stem chordate, or already specialized in the Cambrian? *J. Exp. Zool. B Mol. Dev. Evol.* **320**, 247–271 (2013). doi:10.1002/jez.b.22500 Medline

62. S. C. Morris, J.-B. Caron, *Pikaia gracilens* Walcott, a stem-group chordate from the Middle Cambrian of British Columbia. *Biol. Rev. Camb. Philos. Soc.* **87**, 480–512 (2012). doi:10.1111/j.1469-185X.2012.00220.x Medline

63. S. Zamora, I. A. Rahman, A. B. Smith, Plated Cambrian bilaterians reveal the earliest stages of echinoderm evolution. *PLOS ONE* **7**, e38296 (2012). doi:10.1371/journal.pone.0038296 Medline

64. R. C. Brusca, W. Moore, S. M. Shuster, *Invertebrates* (Sinauer, ed. 3, 2016).

pramolecular network. This component comprises a ureidopyrimidinone (UPy) supramolecular motif that forms long fiber bundles (*8*). Although the UPy motif also interacts with the surfactant, the assembled UPy fiber bundles are not evidently disturbed by the presence of surfactant. By this approach, the system of BTA-EG_4 and surfactant, at concentrations that previously formed a sol consisting of spherical assemblies, can instead form a gel by adding a high concentration of UPy fibrillar structures. Dilution from this initial point surpasses the gelation capacity of the UPy network while not yet reaching the point of inducing BTA-EG_4 filament formation, yielding a sol. Continued dilution activates BTA-EG_4 filament formation, which in combination with the remaining UPy fiber bundles restores a gel state comprising two orthogonal networks of supramolecular polymers: the BTA-EG_4 and UPy networks. Upon further dilution, the system transitions back to a sol once again.

The tunable nature of molecular-scale self-assembly in these materials offers simple synthetic analogues of more complex phenomena observed in nature. For example, membraneless organelles—distinct compartments within a cell that are not enclosed by a traditional lipid membrane—are thought to arise from liquid-liquid phase separation because of concentration gradients of associating multicomponent systems forming these assemblies in a water environment (*9*). The roles of membraneless organelles in biological signaling during both normal and diseased states are increasingly appreciated (*10*). The behavior of the simple systems described by Su *et al.* is therefore reminiscent of more complex self-assembly phenomena in biology, illuminating the importance of subtle thermodynamic driving forces that give rise to concentration-dependent phase separation. This new paradigm in self-assembled materials consisting of highly adaptive and dilution-triggered hydrogels may furthermore lead to the design of stimuli-responsive material platforms for in situ modulation of function in therapeutic biomedicine. ■

REFERENCES AND NOTES

1. M. A. Stuart *et al.*, *Nat. Mater.* **9**, 101 (2010).
2. L. Su *et al.*, *Science* **377**, 213 (2022).
3. T. Aida, E. W. Meijer, S. I. Stupp, *Science* **335**, 813 (2012).
4. M. J. Rosen, J. T. Kunjappu, *Surfactants and Interfacial Phenomena* (Wiley, ed. 4, 2012).
5. K. L. Morris *et al.*, *Nat. Commun.* **4**, 1480 (2013).
6. W. M. Jacobs, D. Frenkel, *Biophys. J.* **112**, 683 (2017).
7. C. M. Leenders *et al.*, *Chem. Commun.* **49**, 1963 (2013).
8. S. I. S. Hendrikse *et al.*, *Chem. Commun.* **53**, 2279 (2017).
9. J. A. Riback *et al.*, *Nature* **581**, 209 (2020).
10. Y. Shin, C. P. Brangwynne, *Science* **357**, eaaf4382 (2017).

ACKNOWLEDGMENTS

M.J.W. acknowledges funding from the National Institutes of Health (R35GM137987) and the National Science Foundation (BMAT, 1944875).

10.1126/science.abo7656

EVOLUTION

"Arch"-etyping vertebrates

Cellular details of gill arches in Cambrian fossils reignite a centuries-old debate

By **Tetsuto Miyashita**

Scientists have long been searching for fossils of distant vertebrate ancestors. In the 1990s, mysterious fishlike forms—now known as yunnanozoans—were discovered at a 520-million-year-old Cambrian fossil site in the Yunnan province of China (*1*–*3*). More fishlike forms (e.g., *Haikouichthys* and *Myllokunmingia*) were reported from the same locality shortly thereafter (*4*, *5*), while the 508-million-year-old Burgess Shale in the Canadian Rockies yielded *Metaspriggina* (*6*). Having eyes and a brain at the front end of an otherwise wormlike soft body, these animals appear to have branched off the phylogenetic tree before the last common ancestor of all living vertebrates. However, there is ongoing controversy about precisely how close to vertebrates these Cambrian forms were. On page 218 of this issue, Tian *et al.* (*7*) present compelling evidence in yunnanozoans for an unmistakable vertebrate trait—a pharyngeal skeleton made of cellular cartilage.

Interpreting organic stains on a shale slab is both a science and an art. Wielding scanning electron microscopy and computed microtomography scans to yield unprecedented details, Tian *et al.* reveal cellular and subcellular structures of the skeletal bars that best compare to cartilaginous gill arches of modern vertebrates. These bars in yunnanozoans are patterned in a series, each associated with gill filaments and connected by horizontal rods. The morphology closely approximates various predictions for vertebrate ancestors.

Of all the internal structures of the earliest vertebrates, pharyngeal skeletons perhaps stand the best chance for fossilization given their robustness. Nonetheless, the complex evolutionary history of the pharynx has

Of gills and jaws

Cambrian vertebrates each evolved distinct pharyngeal anatomy with a series of gill-supporting skeletons. The yunnanozoan has a cartilaginous basket and the *Haikouichthys* has unjoined bars, whereas the *Metaspriggina* has upper and lower rods. However, it remains an open question whether their gill anatomies represent any evolutionary link to the jaws of modern vertebrates.

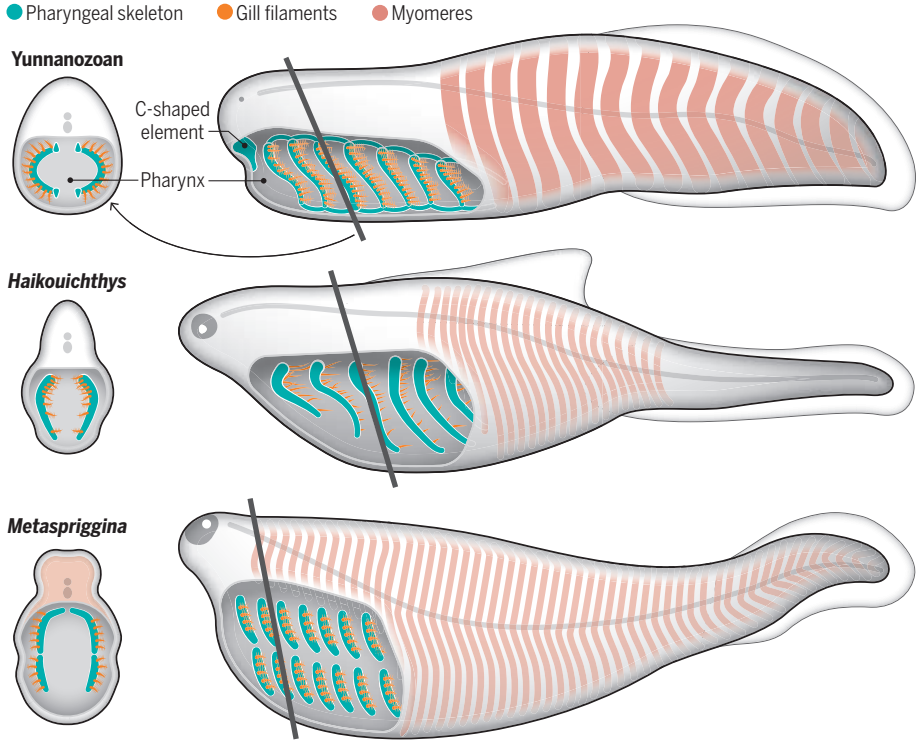

GRAPHIC: V. ALTOUNIAN/SCIENCE

strained attempts to interpret fossil imprints. Pharyngeal slits and skeletons long precede the origins of vertebrates, and cellular cartilage has been found in the lips of a developing invertebrate chordate (*8*). Vertebrates develop the entire pharyngeal skeleton from cellular cartilage in the embryonic pharyngeal arches. This cartilage originates in the vertebrate-specific cell lineage called the neural crest. To complicate matters further, the pharynx is regionally and phylogenetically differentiated among vertebrates. Depending on whether similarities or differences are emphasized, the pharyngeal arch I in which jaws develop, that is, the mandibular arch, may (*9*–*11*) or may not (*12*–*14*) share an evolutionary origin with gill-supporting skeletons. New information from yunnanozoans presents an opportunity to clarify these issues.

Tian *et al*. avoided jumping to conclusions, as they did not explicitly identify which gill bar in a yunnanozoan corresponds to which arch in a modern vertebrate. But they did signal their favored interpretation that yunnanozoans, with each gill bar identical to the next, represent the ancestral vertebrate condition. This view is in line with the belief that all pharyngeal arches originally supported gills and that one of them evolved into a jaw (*9*–*11*). At face value, yunnanozoans could serve as long-awaited evidence for the gill-arch hypothesis of jaw origins.

However, this jaw-origin narrative relies solely on how one chooses to identify the gill bars of yunnanozoans—that is, whether the first gill bar in yunnanozoans corresponds to the mandibular arch in jawed vertebrates. Historically, one or more additional arches were postulated in front of the mandibular arch for vertebrate ancestors (*11*). Other views posit no such extra arches and consider the mandibular arch as distinct from the gill arches (*12*–*14*). Yunnanozoan morphology excludes none of these ideas. Their first gill bar could be the elusive arch that was later lost in vertebrates, or, conversely, the mandibular region might not have formed a full skeletal arch. Consistent with the latter scenario, the snout and lips either appear diminutive or are absent in yunnanozoans and other Cambrian forms (*5*–*7*). Specifically, one C-shaped oral structure, as identified by Tian *et al*., may represent what might be a slim mandibular arch of yunnanozoans. If this is true, then a prominent snout and lips, which arise from the neural crest, are a later innovation of the living vertebrate group.

To discriminate between different hypotheses, unequivocal correlates of arch identities are needed. A mandibular arch is not defined by being the most anterior pharyngeal arch. Rather, its identity is predicated on the presence of a specific stream of neural crest cells, a fifth cranial nerve, and specialized mouth structures for pumping water and feeding. Without these markers, and with variations observed among different vertebrate lineages, overall positions of the gills help little to determine arch homology in yunnanozoans.

Tian *et al*. offer an emerging scope of diversity in pharyngeal anatomy of early vertebrates (see the figure). Among other Cambrian fishlike forms, *Haikouichthys* seems to have skeletal rods that support the gills, whereas only the gill pouches are described for *Myllokunmingia* (*4*). *Metaspriggina* has skeletal bars segmented into upper and lower halves (*6*). Hagfish and lampreys evolved from the common ancestor with a cartilaginous basket around the gill pouches and a specialized oral skeleton (*15*). Similar pharyngeal skeletons also occur in successive out-groups of jawed vertebrates (*12*). And jawed vertebrates have a series of jointed skeletal arches, the first of which differentiate as jaws. These different patterns are as anatomically disconnected from each other as they are phylogenetically distant.

Given such a complex distribution of characters, it seems premature to assume any single form as the ancestral phenotype on a linear path toward modern vertebrates. In the phylogenetic analysis by Tian *et al*., yunnanozoans are an out-group to all other vertebrate branches. This suggests differential evolution of pharyngeal patterning among early vertebrate lineages. By the time yunnanozoans were sloshing about in the Cambrian sea, other primitive fishes had evolved to slurp food differently with their uniquely derived pharyngeal anatomy. Although evolutionary biologists have been busy chasing the mythical ancestor that explains everything about the vertebrate body plan, perhaps the opposite is a sensible approach. In other words, the meandering journey toward modern vertebrates may be best understood by populating the family tree with divergent and discontinuous anatomical forms, guided by phylogenetic inference rather than by theory. ■

Canadian Museum of Nature, Ottawa, Ontario K1P 6P4, Canada. Email: tmiyashita@nature.ca

REFERENCES AND NOTES

1. J.-Y. Chen *et al*., *Nature* **377**, 720 (1995).
2. J.-Y. Chen *et al*., *Nature* **402**, 518 (1999).
3. D. Shu *et al*., *Science* **299**, 1380 (2003).
4. D.-G. Shu *et al*., *Nature* **402**, 42 (1999).
5. D.-G. Shu *et al*., *Nature* **421**, 526 (2003).
6. S. Conway Morris, J.-B. Caron, *Nature* **512**, 419 (2014).
7. Q. Tian *et al*., *Science* **377**, 218 (2022).
8. D. Jandzik *et al*., *Nature* **518**, 534 (2015).
9. J. A. Gillis *et al*., *Nat. Commun.* **4**, 1436 (2013).
10. C. Hirschberger *et al*., *Mol. Biol. Evol.* **38**, 4187 (2021).
11. J. Mallatt, *Zoolog. J. Linn. Soc.* **117**, 329 (2008).
12. P. Janvier, *Early Vertebrates* (Oxford Monographs on Geology and Geophysics, Clarendon Press, 1996).
13. S. Kuratani, *Evol. Dev.* **14**, 76 (2012).
14. T. Miyashita, *Biol. Rev. Camb. Philos. Soc.* **91**, 611 (2016).
15. T. Miyashita, *Can. J. Zool.* **98**, 850 (2020).

10.1126/science.adc9198

NEUROSCIENCE

Sounding out pain

A circuit for sound-induced analgesia has been found in the mouse brain

By **Rohini Kuner**[1] *and* **Thomas Kuner**[2]

The perception of physical pain is subject to variation depending on the context and which other sensory inputs are being received, including sound. The emerging field of music therapy (*1*)—which is applied to control postoperative, pediatric, postpartum, and cancer pain and is being increasingly tested in chronic pain disorders—capitalizes on the interactions between sound and pain perception to attenuate pain. Given that music and natural sounds can positively affect mood, relieve stress, and relax the body, it is not unreasonable to think that these factors underlie pain relief. On page 198 of this issue, Zhou *et al*. (*2*) demonstrate that pain relief by sound is not purely attributable to stress reduction and distraction. They interrogate neural circuits to unravel a specific pathway for sound-induced analgesia in the brains of mice.

Using rodents to study how music and sound are related to pain presents major challenges, not least because it is unknown how animals perceive music. Zhou *et al*. carried out behavioral tests addressing pain sensitivity and found that mice did not show differential responses to melodic classical music (consonant sounds), dissonant music, or white noise. Notably, they found that the decisive factor in eliciting pain relief is a 5-dB increase in sound intensity in any of these three types of sound relative to ambient sound levels, whereas 10-, 15-, or 20-dB increases were ineffective. In mouse models, a 5-dB increase in sound intensity led to inhibition of both sensory-discriminative aspects of pain, such as evoked responses aiding escape from noxious stimuli (nociception), and affective behaviors that are linked to suffering and negative emotions associated with acute and chronic pain. Therapeutically relevant findings were that repetitive application of 5-dB sound over ambient levels

[1]Institute of Pharmacology, Heidelberg University, Heidelberg, Germany. [2]Department of Functional Neuroanatomy, Institute for Anatomy and Cell Biology, Heidelberg University, Heidelberg, Germany. Email: rohini.kuner@pharma.uni-heidelberg.de

“Arch”-etyping vertebrates

Tetsuto Miyashita

Science, 377 (6602), • DOI: 10.1126/science.adc9198